STATIC STABILITY AS AN AID IN NUMERICAL BAROCLINIC-ZONE ANALYSIS

JAMES M. HAMRICK

STATIC STABILITY AS AN AID IN NUMERICAL BAROCLINIC-ZONE ANALYSIS

by

James Murchison Hamrick
Lieutenant, United States Navy
B.S., United States Naval Academy, 1958

[redacted]

Submitted in partial fulfillment
for the degree of

MASTER OF SCIENCE

from the

UNITED STATES NAVAL POSTGRADUATE SCHOOL
May 1966

ABSTRACT

Static stability is investigated as a contribution to numerical baroclinic-zone analysis, developed by Renard and Clarke, and presently being produced on a hemispheric basis by the U. S. Navy at the Fleet Numerical Weather Facility, Monterey, California (FNWF). Significant-level and mandatory-level data from the North American region at 00Z and 1200Z, 20 August 1965, are utilized in an experiment relating 850, 700, 500, and 300-mb static stabilities and associated parameters to a FNWF front-location parameter proportional to horizontal shear of the thermal wind which is dependent on mandatory level data only.

Three methods are used to compute static stability in the form of $\frac{\partial \ln \theta}{\partial \ln p}$, the most promising one involving a parabolic fit of potential temperature to the four mandatory levels. A derivative of static stability is used to locate baroclinic zone boundaries. Finally, the vertical gradient of potential temperature in combination with the slope of isentropic surfaces is used to determine isobaric gradients of potential temperature which yields an analysis of baroclinicity with resolution surpassing that of the present FNWF product.

TABLE OF CONTENTS

TABLE AND ILLUSTRATIONS

TABLE AND ILLUSTRATIONS (cont'd)

TABLE AND ILLUSTRATIONS (cont'd)

ABBREVIATIONS AND DEFINITIONS

1. a, b, c: Constants.
2. A: Degrees absolute.
3. g: Force of gravity.
4. FNWF: United States Navy Fleet Numerical Weather Facility, Monterey, California.
5. GGθ: $=-\frac{\partial^2\theta}{\partial n_\theta^2}$ = FNWF's operational front-location parameter.
6. GSS: A parameter similar to GGθ, defined as $-\nabla SS\cdot\vec{n}_\theta$.
7. Gθ: $=\left|\frac{\partial\theta}{\partial n_\theta}\right|$: Magnitude of the gradient of potential temperature.
8. $\vec{n}_\theta$: The unit vector ascendant directed normal to isentropes on a constant pressure surface.
9. NMC: National Meteorological Center, Environmental Sciences Services Administration, Suitland, Maryland.
10. NPGS: United States Naval Postgraduate School, Monterey, California.
11. P, p: Atmospheric pressure
12. P_θ: Pressure on an isentropic surface.
13. P_u, P_l, P_{ml}: Pressure at the first significant level above a mandatory level, at the first significant level below a mandatory level, and at the mandatory level, respectively.
14. SS: Static stability.

15. Δ ( ): A finite increment of ( ).

16. Δ (Δ P): Error in pressure interval bounded by mandatory and significant levels.

17. Δ ($\Delta\theta$): Error in potential temperature change over interval ΔP.

18. $\Delta G\theta$: $\overline{/}$Computed Gθ (using Equation (11))$\overline{/}$ - $\overline{/}$FNWF's processed G$\theta\overline{/}$.

19. ΔSS: Error in static stability.

20. γ : Lapse rate.

21. γ_d : Dry adiabatic lapse rate.

22. σ : FNWF's static stability parameter.

23. θ : Potential temperature

24. θ_U , θ_L , θ_{mL} : Potential temperature at the first significant level above a mandatory level, first significant level below a mandatory level, and at the mandatory level, respectively.

25. $\left|\frac{\delta p}{\delta n}\right|_{\theta\theta}$: Slope of an isentropic surface.

26. ∇SS: Gradient of static stability.

27. $\nabla\theta$: Gradient of potential temperature.

28. $\frac{\partial\theta}{\partial p}$: Change in potential temperature relative to a change in pressure at constant x, y, t.

29. $\frac{\partial T}{\partial z}$: Change in temperature relative to a change in height ($= -\gamma$).

1. Introduction

Considerable developmental work has been performed at the U. S. Navy Fleet Numerical Weather Facility (FNWF) and the U. S. Naval Postgraduate School (NPGS) on the problem of locating frontal zones by numerical methods. [1, 8, 9] The most promising and currently operational approach utilizes the second derivative of potential temperature $\left(-\frac{\partial^2\theta}{\partial n_\theta^2}\right)$ as a front-location parameter, hereafter referred to as GGθ. Axes of relative minima and maxima in the GGθ fields which bound the baroclinic zones are associated with relative maxima in the horizontal shear of the thermal wind. The axes of relative maxima represent the warm-air boundary of baroclinic zones and, as such, are a numerical form of conventional fronts. These numerical fronts have a close resemblance to hand-analyzed fronts, as may be seen in Figure 1 which shows a typical FNWF operational analysis of GGθ, and Figure 2 which indicates the relation of the numerical front (i.e., GGθ ridge) to the sea-level pressure analysis.[1]

However, recent statistical evaluations indicate a need for improving the numerical product in certain areas, such as in eastern ocean and subtropical regions and frontal occlusions. The author of this study compared

[1]Throughout the subsequent discussion the following terminology is used interchangeably: (a) GGθ fronts, numerical fronts, baroclinic zone boundaries; (b) GGθ ridge, numerical front, warm boundary of baroclinic zone; (c) GGθ trough, cold boundary of baroclinic zone; (d) numerical frontal zones, baroclinic or hyperbaroclinic zones; (e) hand-analyzed fronts, manually analyzed fronts, conventional fronts, NMC fronts.

1000-mb fronts, specified by GGθ, with hand-analyzed surface fronts of the National Meteorological Center, (NMC) for 16 observation times in the late summer of 1965 [4]. It was found that 72% of the GGθ fronts could be associated with NMC fronts. The average distance separating the two fronts was about 90 nautical miles, slightly greater in sparse data areas. These statistics were based on a sample of over 250,000 miles of fronts. Table I recapitulates this and other findings.

In its present operational form, θ is determined from mandatory level data only, however θ or its derivative (Gθ and GGθ) may be computed along any level of meteorological interest (e.g., 1000-mb, earth's surface, 5,000 feet, mean level of 1000/700-mb layer.) It is reasonable to expect that consideration of the detailed temperature structure (i.e., from significant as well as mandatory levels) in the vertical will contribute to the accuracy of locating baroclinic zones at the aforementioned levels.

This study introduces detailed vertical resolution through a static stability parameter computed from significant-level as well as mandatory-level data. The quantity was evaluated, first as an entity unto itself, and later, combined with other quantities to determine frontal locations and intensities. Specifically, the computed static stability field was considered:

(1) Relative to FNWF's operational model of GGθ, as well as to their present static stability evaluation [5, 6]. (See section 4)

(2) As a contribution toward a more detailed GGθ analysis through the introduction of detailed vertical temperature structure. (see section 6)

2. Selection of a Suitable Static Stability Parameter.

Static stability refers to the resistive force offered to motions of

various types by the vertical density structure of the atmosphere in the gravitational field and, specifically, for the atmosphere in hydrostatic equilibrium. Here static stability is proportional to $\gamma_d - \gamma$. When $\gamma_d > \gamma$, an individual air parcel displaced dry adiabatically in a vertical direction will tend to return to its original position, and the air column is said to be statically stable.

Frontal layers are zones of relatively high values of static stability, since within such layers temperature usually deviates from its normal decrease with increasing height to yield isothermal or inversion conditions.

Thus, it appears meaningful to compute static stability for geometric or isobaric levels of interest over an area. Relatively high values of static stability ought to be located within frontal zones and, thus, the static stability should have a high positive correlation with baroclinicity; GGθ ridges and troughs should bound zones of high static stability. Since a large value of stability does <u>not</u> imply the existence of a baroclinic zone, and vice-versa, it is expected that some stability ridges (that is, axes of relative maxima) and numerical fronts may exist independently. Figure 3 shows a low tropospheric vertical cross-section of the eastern Pacific [7]. This cross-section illustrates high values of static stability and baroclinicity in the east Pacific trade-wind inversion east of 135W, while also indicating an area of poor correlation between baroclinicity and stability in the inversion west of 135W.

Gates has made an analysis of advantages and disadvantages of several forms of static stability [8]. Selection of an optimum stability parameter for this project was based on several self-imposed requirements:

(1) static stability will be computed on constant pressure surfaces[2]; (2) the measure should have equal, or nearly equal, values at different levels when γ is the same fraction of γ_d ; (3) static stability should be zero when $\gamma = \gamma_d$; (4) input parameters should be readily available from radiosonde data; and, (5) the computation must readily lend itself to both manual and numerical analysis, the latter currently existent or planned for the future. Requirements 1, 4, and 5 are self explanatory. Requirements 2 and 3 are necessitated by a desire to have comparative fields of static stability at the levels investigated.

A relatively simple, non-dimensional measure possessing the desirable properties is:

$$SS = -\frac{p}{\theta}\frac{\partial \theta}{\partial p} \qquad (1)$$

This measure meets the above requirements very well, moreover, it is directly proportional to $\gamma_d - \gamma$. Gates found that SS computed by this method showed a slight decrease with height up to 300-mb, followed by an increase, but the range of this variation is small and will not be of any consequence here. Equation (1) also portrays the stratosphere realistically, and shows the relatively unstable upper troposphere in both summer and winter.

3. Area and Time of Experiment.

The area and time selected for computing SS were all of the United States, Canada, and Alaska at 00Z and 12Z 20 August 1965. The reported

[2]The present FNWF operational frontal model utilizes mean θ and its derivatives for the layer 1000/700-mb as the basic frontal parameter. Derivatives are computed at constant pressure. (See Figures 1, 2)

radiosonde temperature data were then utilized in three different methods to compute values of SS, for each of approximately 100 reporting stations, at 850, 700, 500, and 300-mb.

20 August 1965 was a well documented day, with extensive data readily available from listings provided by FNWF. The date was marked by the presence of a strong cold front and large stability over the eastern and southern United States. As Gates pointed out, wintertime situations give greater stability contrasts (up to 50%), especially in the lower troposphere, and better delineate frontal zones, but 20 August proved to be quite satisfactory for a pilot project.

4. Computation and Areal Analysis of Static Stability.

I. Methods for Computing Static Stability.

a. Method A. This method consists of computing the stability for the two significant layers[3] adjacent to a mandatory level and plotting the larger of these two values on the appropriate constant pressure chart (850, 700, 500, and 300-mbs.) This approach has the desirable effect of sharply defining the stable baroclinic zone boundaries by assigning to the mandatory level the highest possible SS value from one of the two adjacent significant layers. Figure 4 shows a portion of a typical sounding for which SS might be computed using Method A. Since layer AB is more stable than layer BC, SS is computed for AB and this value is assigned to 500-mb, the mandatory level. Here, the 500-mb level represents the warm-air boundary

[3]A significant layer is bounded by two significant levels, one or both of which may be mandatory levels as well.

of a stable and, presumably, baroclinic zone. Thus a maximum stability value found in a layer within the stable zone is placed at its boundary.

Stability within the significant layer was computed according to the definition in Equation (1). P and θ are the median values for the layer, while the layer value of $\frac{\partial\theta}{\partial p}$ is approximated by $\frac{\Delta\theta}{\Delta p}$ of the layer. In this method, a significant layer was defined as being bounded by a mandatory level and its nearest significant level, regardless of the layer's depth. In another method to be discussed later, layers of less than 10-mb thickness were ignored.

A Fortran 60 program[4] was written to compute stability to four significant figures by this method. The values were rounded to three significant figures and plotted and contoured on FNWF's 1:30 million polar steoreographic projection. Resulting analyses appear as Figures 5-8, with comments on the technique appearing in Appendix I.

Figure 6 (see station 206) displays the merit of this approach, since large gradients of stability do allow the stable zone boundaries to be easily located in this case.

But Method A was not considered satisfactory for several reasons. First, it must be remembered that the objective is to compute stability at the mandatory levels. This system arbitrarily assigns a layer value as the mandatory-level value. The actual value at the mandatory level approaches this arbitrary value as a limit, but for many stations this method gave the

[4]This and all subsequent programs were run on the NPGS's Control Data Corporation 1604 digital computer.

stability for a small layer near the mandatory level, which is not necessarily representative of stability at the mandatory level.

Secondly, this method introduced vertical variation into horizontal gradients of SS. Figure 9A shows a hypothetical case in which SS is higher in the significant layer above station A than in the significant layer below station B. The resulting field of SS tends to give excessive, unrealistic gradients of SS within the baroclinic zone, as well as suggesting improper boundaries of the zone. This problem is magnified for stable zones which are thin (less than 20-mb in depth) and undergo marked variations in depth over small horizontal distances.

Thirdly, it will be noted from a discussion of Methods B and C, that the latter give a more meteorologically satisfying field of SS relative to GGθ baroclinic zones and the hand-analyzed fronts of NMC.

Consequently this method did not look as promising as Methods B and C, and was not further developed.

b. Method B also utilized Equation (1) for each of the four mandatory levels of interest by employing a mathematical best fit of θ at the mandatory level, using transmitted radiosonde data. This data consists of temperature and pressure recorded at each significant level (level where a significant change in temperature lapse rate occurs), as well as for all mandatory levels. Thus the sounding, as plotted from transmitted data, is discontinuous at each of these levels. However, analysis of radiosonde data, assuming every temperature contact is a significant level, indicates the transmitted discontinuity points are largely manufactured by coding and

processing procedures. Thus, fitting a continuous curve to the transmitted sounding for the purpose of obtaining $\frac{\partial\theta}{\partial p}$ is reasonable and justified [2]. This is accomplished by numerically solving the following system of simultaneous linear equations for each sounding:

$$\begin{aligned} \theta_u &= a + bp_u + cp_u^2 \\ \theta_{mL} &= a + bp_{mL} + cp_{mL}^2 \\ \theta_L &= a + bp_L + cp_L^2 \end{aligned} \tag{2}$$

A Fortran 60 program using a Jordan 2 subroutine was written to solve this system for the constants a, b, and c, since all six pressures and temperatures (hence, θ) are known from the sounding.

At the mandatory level, the vertical gradient of potential temperature, $\frac{\partial\theta}{\partial p}$ becomes

$$\frac{\partial\theta_{mL}}{\partial p_{mL}} = b + 2cp_{mL} \tag{3}$$

Thus, Equation (1) was numerically evaluated for

$$SS_{mL} = -\frac{p_{mL}}{\theta_{mL}} \times \frac{\partial\theta_{mL}}{\partial p_{mL}} = -\frac{p_{mL}}{\theta_{mL}}(b + 2cp_{mL}) \tag{4}$$

It can be shown (Appendix III) that the finite difference form of $\frac{\partial\theta_{mL}}{\partial p_{mL}}$ is:

$$\frac{1}{\Delta p}\left[\frac{\Delta p_u}{\Delta p_L} \times \Delta\theta_L + \frac{\Delta p_L}{\Delta p_u} \times \Delta\theta_u\right] \tag{5}$$

This expression was used to manually check computerized results of Equation (4). One such computation appears in Appendix II.

For FNWF numerical operational purposes, Equation (5) would undoubtedly prove to be a more desirable system than Equation (3).

Computed static stabilities were plotted and contoured at a .05 interval, similar to values resulting from Method A.

Two problems appeared at this point: (a) the existence of some negative values of SS on each chart (i.e., absolutely unstable conditions) which verified to be real and representative of low level summer conditions, and,thus, were accepted; and (b) a few questionable values which caused irregularities in otherwise smooth contour patterns. Re-examination of sounding data revealed that a majority of these questionable values of SS resulted when a significant level was located within 10 mb of a mandatory level.

When thin layers of a few millibars are considered, normal errors in pressure and potential temperature can vary the value of SS at the mandatory level by a large percentage. This problem is discussed more fully under Method C.

Furthermore, layers of a few millibars' thickness may be considered mesoscale in character and not sufficiently deep to define synoptic scale frontal layers, or, alternately, as nearly horizontal, thin, stable layers whose relation to baroclinic zones is unexpectedly poor. For example, near 700-mb, a 10-mb layer (about 400 feet) representing a narrow baroclinic zone 100 miles wide, yields a 1/1500 slope. Since baroclinic zones as depicted by GGθ average almost 300 miles, a thin layer (10 mb or less) is, for all practical purposes, horizontal. (Figure 10)

By ignoring layers of 10 mb or less, this system would be throwing out only the nearly horizontal stable layers.

A third method has now been suggested, one which does not consider layers of less than 10-mb thickness adjacent to a mandatory level. This is Method C, discussed below. Since Method A altered 58 out of a possible 440 values computed in Method B, taking all four levels into account, the location of SS ridge lines differed for each method, but contour patterns were basically the same. For this reason, the contour analysis by Method B was not included in this paper. Instead, Figures 11-14 compare the locations of the SS ridge lines produced by Methods B and C. These figures are discussed in Appendix II. On each chart, SS values are shown for all stations where SS varied depending upon the method used. The number plotted above the station is the value computed by Method B; the number below the station is Method C's result. It is evident that the choice of methods heavily influences the location of ridge lines, and the choice of a minimum significant-layer thickness can be a critical factor in locating SS zones.

c. Method C. This method is considered as best representing SS at the four levels of interest. It is identical to Method B, with one exception. Layers 10 mb and less in thickness are considered unrepresentative. In cases where a significant level exists within 10 mb of a mandatory level, the next lower or higher significant level is substituted. For example, assume the levels of interest are 886, 858, 850, and 795 mb. For 850-mb analysis, 858 mb would be ignored since it is within 10 mb. Instead of

858 mb, 886 mb and its associated temperature are substituted for P_u and T_u.

Thus, Method B is a very precise method, taking every fluctuation of temperature in the layers surrounding the mandatory levels into account. Method C includes a small "smoothing factor", which has the effect of filtering out some of the "noise" created by very thin (i.e., non-synoptic scale) layers. Furthermore, the minute temperature changes in thin layers dictates use of layers thicker than 10 mb, primarily because of the accuracy demanded by this method.

When compared with FNWF numerical fronts for the same time and level, the more satisfying appearance of the SS ridges using Method C raises the question as to the best smoothing factor to be employed. Perhaps raising the minimum thickness of the significant layer to 20 mb may even be justified. An error analysis of SS brings out this point. Considering an error in static stability (ΔSS) at a mandatory level as a function of errors in significant layer depth $\overline{\Delta\ (\Delta P)}$, and temperature change in the layer $\overline{\Delta\ (\Delta \theta)}$, Equation (1) may be differentiated to obtain:

$$\Delta SS_{mL} = -\left[-(\Delta\theta)(\Delta p)^{-2}\ \Delta(\Delta p) + \Delta p^{-1}\ \Delta(\Delta\theta)\right] \frac{\rho_{mL}}{\theta_{mL}} \qquad (6)$$

Probable errors in pressure and temperature are assumed to be 1 mb and 1°C, respectively, in the low troposphere $\overline{1}\overline{1}$. So as not to inflate the proposed error, it may be assumed the probable error occurs at only <u>one</u> boundary of the significant layer, errors in θ and T are the same magnitude, and transmission errors are excluded. Further, assuming P = 700-mb,

$\theta = 310^{\circ}$, and $\Delta\theta = .2^{\circ}C$ for each ΔP interval of 2 mb, the following results:

ΔP(mb)	$\Delta\theta(^{\circ}C)$	Δ SS
2	.2	104%
10	1	21%
20	2	11%

Thus, dramatic changes in accuracy are achieved by proper selection of the smoothing factor, while still retaining the desired vertical resolution. Further experimentation is certainly warranted before final selection of the optimum minimal thickness of significant layers.

d. Analysis Techniques Employed with Method C Data.

Data obtained by Method C were plotted on 1:30 million polar stereographic charts and analyzed for 00Z and 12Z 20 August at all four levels. (Figures 15-24)

Any attempt to contour an area as large as the United States, Canada, and Alaska on the basis of about 100 observations is open to criticism, since any one of several interpretations may be used without violating data. This is especially true in Canada, where extensive sparse data areas exist. The proper orientation of the isolines of SS is intrinsic to proper location of the ridge line of SS. Since the ridge line suggests the location of the frontal zone and/or its boundaries, an assist or first guess was sought for the SS analysis.

Since the ultimate goal of this project is to guide, or even replace, the present FNWF system of frontal analysis, it was considered valid to use the GGθ field as an aid in contouring SS by orienting the SS lines parallel to the numerically computed baroclinic zone boundaries

wherever data allowed. It turned out that forcing was not necessary, since SS isolines did indeed parallel baroclinic boundaries on most occasions, especially in areas of strong baroclinicity. The result looks very promising, since the patterns obtained show a striking resemblance to GGθ ridge lines, notably at 850 and 700 mb. (Figures 15, 16, 20, and 21)

II. Discussion and Evaluation of SS Charts Produced

At this juncture it was felt that Method C, considering baroclinic zones presented SS in its most palatable form as representative of frontal phenomena. The only obvious shortcoming is its subjectivity, being a manually produced analysis product.

Appendix III contains a detailed analysis of eight charts, one for each level of interest for both 00Z and 1200Z 20 August 1965, the charts appearing as Figures 15-18 and 20-23. Speaking in general terms, it can be observed that:

a. Most ridge lines of SS are in close proximity to NMC fronts and to ridge lines of GGθ; exceptions are manifest at higher levels (500 and 300-mb), and in mountainous areas.

b. There are more miles of SS ridge lines than GGθ fronts, and more GGθ fronts than NMC fronts, the latter fact indicated in /1/ and /4/.

c. SS ridge lines have obvious vertical consistency between the 850 and 700-mb levels, especially over the dense data, non-mountainous region of North America, where a hand-analyzed front also exists. Here, the 700-mb front trails its 850-mb counterpart by about 100 miles. This

seems consistent with the normal slope of a low tropospheric front. In the same area, the 500-mb SS ridge trails the 700-mb position by as much as 300 miles (Great Lakes area, 1200Z) and it is at this level that vertical continuity breaks down. Not all fronts reach the 500-mb level, and of those that do, many show a sharply decreased slope. Such an observation is in agreement with findings by other investigators [10]. Vertical consistency of SS ridges in mountainous regions, sparse data areas, and the peripheral map area is fair to poor.

d. The ridge lines at 300-mb are questionable representatives of low troposphere fronts for the same reasons outlined above. There is the additional problem posed by the tropopause. In computing SS by Method C, data up to 250-mb were often used. In winter, the low-level tropopause gives high stabilities over some mid-latitude stations, and thus gives a false indication of a front. Several soundings in Canada (stations 722, 909, 913, 915, 917, and several others) indicated a tropopause existing between 250- and 300-mb

e. The ridge lines of SS showed good time continuity in the area of good vertical consistency.

f. In areas of sparse data, subjectivity enters the analysis. In areas where three or four reports determine the contour pattern over an area of thousands of square miles, baroclinic zones, history, and vertical consistency are the only aids available. These are important considerations when viewing application on a hemispheric scale, utilizing computerized solutions.

III. Comparison of SS with FNWF's Static Stability Analysis (σ).

a. Observations:

FNWF's data processing program produces mean static stability for five layers (σ) [5,6]. Such a computation, of course, was not meant for aid in frontal analysis. However, it is pertinent to this investigation to compare the merits of SS computed for a level, using the maximum vertical resolution, with σ, computed for a layer using mandatory level information only. A detailed comparison of the two analyses appears in the comment section of Appendix IV. The discussion here is limited to the following general observations.

The use of mandatory level data only gives a gross picture of stability, and says little about stability at a particular level. A frontal layer could be embedded within the 775/600-mb layer, and mandatory level data might never detect it. On the other hand, SS using significant as well mandatory level data is more representative, if for no other reason than the increase in data and the vertical resolution.

SS has the added advantage of being computed for four specific constant pressure surfaces in the atmosphere. With the wide use of 850-, 700-, and 500-mb charts, stability computed at a level is more meaningful than stability within a gross layer.

b. Conclusions:

When compared with FNWF's σ analysis, SS is a more meaningful representation of frontal zones because of:

(1) the use of actual data from radiosonde reports vice processed data as used by FNWF.

(2) the high vertical resolution resulting from the use of significant vice mandatory level data.

(3) the improved accuracy derived from using a parabolic fit of potential temperature at the mandatory level with no assumption about the vertical gradient of static stability.

IV. Recommendations on SS.

Based on the aforementioned findings, the following recommendations are made relative to further testing and application to frontal analysis:

a. Limit the mandatory levels to the 850-, 700-, and 500-mb surfaces for low tropospheric frontal phenomena.

b. Compute SS as indicated by Method C.

c. Statistically compare SS ridges with computer and hand-drawn fronts and baroclinic zones produced by NMC and FNWF, respectively.

d. Consider programming computation of SS on a hemispheric basis, say in the framework of the data processing scheme at FNWF. It is realized that this requires, apriori, a suitable data-handling program in order to marry the mandatory and significant level radiosonde data. Presently, the significant level data are copied on tape but not read out or utilized in any way in FNWF's automatic data processing program.

e. Subsequent to d, analyze the SS field considering it or its derivatives as an adjunct to the GGθ analysis for locating baroclinic zones.

f. Investigate the feasibility of computing SS for the surface, or 1000 mb, by assigning the SS computed for the lowest significant layer (or level) as the value at the surface.

5. The Gradient of Stability: GSS.

I. Definition of Parameter.

As indicated in the Introduction, FNWF's present operational product for frontal analysis is the GGθ field. This field, as defined by Renard and Clarke, is the directional derivative of the gradient of potential temperature along its gradient [8]. In mathematical terms:

$$GG\theta = -\nabla|\nabla\theta| \cdot \frac{\nabla\theta}{|\nabla\theta|} \equiv -\nabla|\nabla\theta| \cdot \vec{n}_\theta \equiv -\frac{\partial^2\theta}{\partial n_\theta^2} \qquad (7)$$

Referring to SS and recalling that it is already a first derivative, a similar expression involving stability may be written:

$$GGS = -\nabla SS \cdot \frac{\nabla\theta}{|\nabla\theta|} \equiv -\nabla SS \cdot \vec{n}_\theta \qquad (8)$$

The GGθ and GSS fields are entirely similar in gross features, as may be seen by Figure 25.

II. Discussion of Procedure.

GSS was calculated manually for the 700-mb level for 00Z 20 August 1965. The mechanics of this calculation were as follows:

a. Using FNWF's hemispheric printout of potential temperature at 700-mb, $\vec{n}_\theta$ was determined at each grid point over the area of interest.

b. For each grid point, the gradient of stability was determined using $\frac{\Delta SS}{\Delta \vec{n}_\theta}$, where $\Delta \vec{n}_\theta$ was taken as 120 nautical miles, with the grid point at the centrum. This distance is rather arbitrary, being

selected mostly on the basis of allowing for a well defined field of GSS. In other words, the larger the distance $\Delta\vec{n}_\theta$, the flatter the field of GSS.

c. GSS was plotted on a 1:30 million polar stereographic projection and then analyzed. This chart appears as Figure 25. The warm air boundary of a baroclinic zone is associated with the ridge or axis of a relative maximum in GSS, while the cold air boundary is representative of the trough or axis of a minimum is GSS.

III. Conclusions.

a. GSS does appear to offer some advantage over the SS field for frontal information. SS defines a ridge only, which is associated with the centrum of the zone, while GSS defines a ridge and a trough which outline the boundaries of the baroclinic zone. In comparing these boundaries with the baroclinic zone limits derived from GGθ, the GSS boundaries define a zone which averages about 100 miles narrower than GGθ, except over the west central U. S. (See Figure 25) There are at least two reasons for the suggested narrower baroclinic zones:

(1) greater vertical resolution in computed GSS vs. GGθ from FNWF; or

(2) use of 120 miles to compute GSS instead of several grid lengths, as used by FNWF.

b. The manual computation of GSS is a time consuming process, requiring about three hours to produce the 700-mb chart for the North American area. However, the computation of GSS is adaptable to the computer, the mechanics of the operation being almost identical to the computation of GGθ.

IV. Recommendations.

a. If GSS is investigated at some later date, the procedures outlined in this section are recommended, but it is suggested that the entire operation be programmed with GSS as the final product.

b. If the above recommendation is carried out, statistically compare GSS with GGθ to determine if the former is consistently better in outlining the baroclinic zones.

c. The following section concerns an alternate approach to obtaining baroclinic zone boundaries. Since SS and GSS experiments were but pilot projects, it is recommended that a more exhaustive study be made relating the GSS scheme to the approach in the next section.

6. Gθ Computed Using High Vertical Resolution.

I. Definition of Parameter.

As discussed in Section 3, GGθ in its present operational form utilizes mandatory level data only for frontal analysis.

Consider the following:

If $\theta = \text{fcn.}(p, n_\theta)$

$$d\theta = \frac{\partial \theta}{\partial n_\theta}\delta n_\theta + \frac{\partial \theta}{\partial p}\delta p \qquad (9)$$

Next, set $d\theta = 0$ for purposes of computing the slope of an isentropic surface, here, in the direction of maximum slope. Thus,

$$\left|\frac{\delta p}{\delta n_\theta}\right|_\theta = -\frac{\partial \theta}{\partial n_\theta} \Big/ \frac{\partial \theta}{\partial p} \qquad (10)$$

$$\text{and, } -\frac{\partial \theta}{\partial n_\theta} = \left|\frac{\delta p}{\delta n_\theta}\right|_\theta \times \frac{\partial \theta}{\partial p} \qquad (11)$$

$$\text{where, } G\theta = \left|-\frac{\partial \theta}{\partial n_\theta}\right| \qquad (12)$$

$$\text{Finally, } GG\theta = -G(G\theta) = -\frac{\partial^2 \theta}{\partial n_\theta^2}$$

II. Discussion of Procedure.

Equation (11) can be solved from available data since $\frac{\partial\theta}{\partial p}$ may be computed using Method C, and $\left|\frac{\delta p}{\delta n_\theta}\right|_\theta$ can be determined utilizing FNWF's hemispheric printout of P_θ. Thus, a $G\theta$ results which incorporates the high vertical resolution inherent in the use of significant level data through consideration of $\frac{\partial\theta}{\partial p}$. This new $G\theta$ may then be compared with FNWF's hemispheric printout of $G\theta$ to determine whether high vertical resolution used in this fashion enhances the operational frontal product.

The mechanics of determining $\left|\frac{\delta p}{\delta n_\theta}\right|_\theta$ involved obtaining hemispheric printouts of P for each 2.5 A of potential temperature from 280A to 330A, in order to compute $-\frac{\partial\theta}{\partial n_\theta}$ at 850 and 700-mb. for 00Z 20 August 1965. $\left|\frac{\partial\theta}{\partial n_\theta}\right|_\theta$ was computed at each station, using a centered finite difference scheme applied to two mesh lengths of the FNWF grid. Interpolation of $\left|\frac{\delta p}{\delta n_\theta}\right|_\theta$ for the exact θ surface was made, as appropriate. Finally, the products of $\left|\frac{\delta p}{\delta n_\theta}\right|_\theta$ and $\frac{\partial\theta}{\partial p}$ were obtained for each station at 850 and 700-mb. The resulting values of $G\theta$ (hereafter referred to as <u>computed Gθ</u>) were transferred to 1:30 million charts and compared with FNWF's $G\theta$ values.

III. Results.

The comparison between computed and FNWF $G\theta$ values appears in tabular form as Appendix V. Note that computed $G\theta$ has been used as the basis, since its values are correct to three significant figures, and its use allows the selection of 177 specific reference points (considering both charts) for comparison of the values.

Each chart was arbitrarily separated into two parts, for reasons which will soon become evident. One part was the baroclinic zone, which was defined here as the area enclosed by the $1.0^{\circ}C/100$ km. isoline.[5] The remaining area was simply considered outside the baroclinic zone. Figures 26 and 27 show a comparison of the baroclinic zones from computed and FNWF $G\theta$ values.

The table in Appendix V reveals that computed $G\theta$ gives relatively higher values in baroclinic zones and lower values outside the zones. This fact is obvious when one notes that of 51 reference points within the baroclinic zone, $G\theta$ is less than $-.2^{\circ}C/100km$ at two points only; while of 126 reference points outside the baroclinic zone, only three values of $\Delta G\theta$ are above $+.2^{\circ}C/100km$.

Thus, as shown by the medians obtained for each area, computed $G\theta$ gives a wider range of values overall, implying a sharper change in gradient (i.e., $GG\theta$) across the boundaries of the zones.

The 16 observations at 850-mb in which the FNWF $G\theta$ exceeded computed $G\theta$ by more than $1.0^{\circ}C/100km$ fell mostly in the southwest desert area of the United States, as may be inferred from Figure 26. As stated in Section 1, this area poses a problem for numerical frontal analysis by $GG\theta$ in that fronts are indicated where none exist in manual analyses, especially in the summer. Computed $G\theta$ has markedly low values in this area. Thus, either the vertical resolution of $\frac{\partial\theta}{\partial p}$ or the use of a three-point vice a

[5]Values on both charts ranged from nearly 0 to $3.0^{\circ}C/100$ km. with two isolated higher values on computed $G\theta$: $5.15^{\circ}C/100km$ at station 764 and $3.50^{\circ}C/100$ km at station 518.

five-point derivative in computing $\frac{\partial f}{\partial n}$ has, at least for this map time, resolved an area of difficulty.

A final result concerning locations of relative maxima and minima in the field show that of 23 relative maxima on the computed $G\theta$ field, there were 17 maxima on FNWF's printout which fell within one mesh length. Of 29 relative minima, FNWF's printout indicated 23 minima within one mesh length. These facts, combined with a cursory glance at Figures 26 and 27, show a similarity of contour patterns, except over the southwest U. S. at 850-mb.

IV. Conclusions.

It is difficult to make any sweeping statements about $G\theta$ computed by Equation (11) on the basis of one map time, but the following comments certainly appear justified:

a. There is a resemblance in the shape and location of baroclinic zones defined by the two methods, especially the warm air boundary.

b. Computed $G\theta$ defines a narrower baroclinic zone with higher values inside and lower values outside the zone.

c. Computed $G\theta$ seems to eliminate the troublesome area over the mountainous and desert southwest at 850- and 700-mb.

Thus, computed $G\theta$ appears to show considerable promise, especially in light of b. and c. The question reduces to an analysis of Equation (11) and a decision as to whether the vertical resolution obtained by the use of significant level data has narrowed and sharpened the

baroclinic zone, or whether the use of a three-point vice a five-point derivative is responsible. Comparisons made by Associate Professor R. J. Renard of the U. S. Naval Postgraduate School and Leo C. Clarke of FNWF, Monterey, California, revealed that the five-point method actually gives a stronger gradient than the three-point. Thus, it certainly appears that $\frac{\partial \theta}{\partial p}$ plays a dominant role in statement b.

As a test, three stations at 700-mb were arbitrarily selected and a comparison made between the three-point (two mesh lengths) derivative used in this experiment and the five-point technique presently used operationally by FNWF. The five-point derivative is described by the quartic interpolation polynomial

$$\frac{\delta p}{\delta n_\theta} \text{ AT } i=0 = \frac{1}{12d}\{(p)_{i-2} + 8[(p)_{i+1} - (p)_{i-1}] - (p)_{i+2}\} \qquad (13)$$

Where d= mesh length = 381km. at 60° latitude, i = 0 is the station location, $i \pm 1$ and $i \pm 2$ are locations one and two mesh lengths from the station, respectively, in a direction normal to isobars on a constant θ surface. The table below suggests that the gradients computed by the two methods are similar, but certainly not the same.

$\delta p / \delta n_\theta$ (mb/100km)

Station	three -points	five-points
712	32.8	29.3
722	40.6	45.9
311	22.3	14.6

V. Recommendations.

Continue experimentation on computed $G\theta$ by:

a. programming the computer to produce $\frac{\delta p}{\delta n_\theta}$ from P_θ charts and multiplying the result by $\frac{\partial \theta}{\partial p}$ from Method C;

b. operate on computed Gθ to get GG0 (this is already an operational procedure at FNWF) with high vertical resolution;

c. make a detailed statistical comparison of the two GGθ parameters to determine which product best delineates the baroclinic zone and its associated frontal phenomena.

7. General Conclusions and Recommendations.

In view of the stated conclusions in each section, only a brief overall review will be given here.

This entire study utilizes data from two map times and attempts to show the value of using significant as well as mandatory level data as a contribution toward numerical baroclinic zone and frontal analysis. Three different parameters for frontal analysis have been presented: SS, GSS, and a computed Gθ. It is not the purpose of this investigation to select from these three a single proposal which is considered best. All three have strong and weak points, and a statistical study covering several periods of time in at least two seasons would be required to make an intelligent selection.

It does appear, however, that the detailed thermal structure of the atmosphere in the vicinity of the mandatory levels can be better visualized by use of significant level data, and that the computation of $\frac{\partial \theta}{\partial p}$ using a parabolic fit is a most promising approach.

8. Acknowledgments.

The writer wishes to express his sincere appreciation to Associate Professor Robert J. Renard of the U. S. Naval Postgraduate School for his guidance and assistance in this project. Appreciation is also expressed to the staff at FNWF and Mr. Leo C. Clarke, in particular, for advice and assistance in obtaining computer products. Other members of the Department of Meteorology and Oceanography, U. S. Naval Postgraduate School, and Weather Records Center at Asheville, North Carolina, are thanked for their cooperation in furnishing data and technical assistance.

BIBLIOGRAPHY

1. Clarke, L. C. and Renard, R. J. "The U. S. Navy Numerical Frontal Analysis Scheme: Further Development and a Limited Evaluation." Unpublished Manuscript, Department of Meteorology and Oceanography, U. S. Naval Postgraduate School, Monterey, California, 1966. (To be published in Journal of Applied Meteorology)

2. Danielsen, E. F. "The Laminar Structure of the Atmosphere and its Relation to the Concept of the Tropopause." Archiv fur Meteorologie, Geophisik und Bioklimatologie, v.11, #3, 1959.

3. Gates, W. L. "Static Stability Measures in the Atmosphere," Journal of Meteorology, v. 18, 1961: 526-533.

4. Hamrick, J. M. "A Frontal Comparison Between a Hand-Analyzed Product and a Numerical Product." Unpublished manuscript, Department of Meteorology and Oceanography, U. S. Naval Postgraduate School, Monterey, California, 1965.

5. Holl, M. M., Bibbo, J. P. and Clark, J. R. "Linear Transforms for State-Parameter Structure." Technical Memo #1, Meteorology International, Inc., Monterey, California, 1963.

6. Holl, M. M., Bibbo, J. P. and Clark, J. R. Supplement to Technical Memo #1, "Linear Transforms for State-Parameter Structure." Meteorology International, Inc., Monterey, California, 1964.

7. Neiburger, Morris, Johnson, D. S. and Chien, Chen-Wu. Studies of the Structure of the Atmosphere Over the Eastern Pacific Ocean in Summer. University of California Press, 1961.

8. Renard, R. J. and Clarke, L. C. "Experiments in Numerical Objective Frontal Analysis," Monthly Weather Review, v. 93, 1965: 548-556.

9. Renard, R. J. and Clarke, L. C. "Present Status of the U. S. Navy's Experiments in Numerical Objective Frontal Analysis and Prognosis." Paper read at the American Meteorological Society Conference on Modern Methods of Weather Forecasting and Analysis, Chicago, Illinois, 23-25 March 1966.

10. Saucier, W. J., Principles of Meteorological Analysis, University of of Chicago Press, 1955.

11. United States Weather Bureau, Synoptic Meteorology as Practiced by the National Meteorological Center. The NAWAC Manual, NAVWEPS 50-1P-548. Washington: Government Printing Office, 1960.

TABLE 1

EVALUATION ANALYSIS

FNWF (NUMERICAL) 1000-MB vs NMC (MANUAL) SFC FRONTS

Dates: 16 obsn. times in period 23 Aug - 6 Sept 65

FNWF FRONTS: 259,000 n.mi.

NMC FRONTS: 284,000 n.mi.

% FNWF FRONTS assoc. with NMC FRONTS: 72%

% NMC FRONTS assoc. with FNWF FRONTS: 66%

Sector	Frontal Distance (n.mi.)	Average Difference (°lat) (FNWF vs NMC) Summer	Winter[6]
North America	49,250	1.6	1.4
Atlantic	46,900	1.4	1.8
Pacific	46,300	2.1	2.3
Europe-North Africa	26,000	1.8	---
Asia	18,000	1.2	---

[6] See [1]

APPENDIX I

SS Analysis by Method A

Technique and Criteria.

SS computations by Method A were plotted on 1:30 million polar stereographic paper and the resulting contour analysis appears as Figures 5-8. Values of SS vary from slightly negative to +.6, with most values falling in the +.05 to +.3 range. Contour interval has been arbitrarily set at .05 for values from 0 to .2, and at .1 thereafter.

Contours of SS are generally elongated and elliptical, somewhat resembling a jet stream analysis. The elongation generally appears parallel to ridge lines.

Ridge lines are drawn only for relative maximum values greater than .1 and then only if more than one station shows such a magnitude. Ridges are also omitted for areas of weak gradient (although values of SS may exceed .1) as well as when considerable subjectivity is required in locating the ridge. Although this discussion concerns Method A, the principles apply to every analysis attempted in this experiment.

850-mb 00Z 20 August 1965. (Figure 5)

It will be recalled from Section 4 that Method A has the advantage of producing numerical values of SS which are somewhat higher than those computed by the other methods discussed herein. These higher values have produced a ridge over the eastern U. S. which is well defined by high SS at stations 712, 528, 520, 429, and 403. This ridge has not been connected to the ridge over the central U. S. because of low SS at station 327, but a

slight relaxing of criteria could have allowed such a marriage. The other three ridges on this chart are a function of a very few station reports, and exact placement was difficult.

The western U. S. has few contours because many of these stations are at pressures greater than 850-mb. The zero contours in the U. S. southwest desert region bounds areas of absolutely unstable lapse rates.

The overall pattern has some resemblance to the frontal patterns achieved by other methods (see Figure 15), but it is clear that correlation is too poor for a comparative analysis to be of any value.

700-mb 00Z 20 August 1965. (Figure 6)

This chart is characterized by several high values of SS which dictate the location of ridge lines. Most of these values are computed from thin layers adjacent to the 700-mb level, and the overall pattern shows very poor correlation with patterns produced by later methods and operational products. (see Figure 16) The most striking example appears at station 206. Other computations modify this 1.86 reading to a value of about .1, a remarkable change. The same criticism can be made of stations 722, 907, and 913.

With the exception of the ridge over the eastern U. S., vertical continuity with the 850- and 500-mb levels is poor.

500-mb 00Z 20 August 1965. (Figure 7)

The 500-mb chart, when compared to GGθ and later methods in this study (Figure 17), has the highest correlation of any chart of the series, showing a long ridge of SS from SE Canada, across the central U. S.,

then north into central and northern Canada. High SS values at stations 520, 712, 747, and 913 dictate the position of the ridge, just as they do in Figure 15. The ridge over the eastern seaboard is well defined, but its position is not verified by any other method. A large portion of the western U. S. exhibits moderately high values of SS, but the area is so broad and the gradient so flat that it is not possible to draw a realistic ridge line.

300-mb 00Z 20 August 1965. (Figure 8)

The pattern at 300-mb is random and irregular. The only ridge showing vertical continuity with lower levels is the ridge over eastern Canada and the east-central U. S. As indicated in the text, there is evidence to support the claim that the 300-mb analysis may not be an aid to lower troposphere frontal analysis. Its value as a front-locator is, therefore, questionable.

APPENDIX II

Comparison of SS Ridge Lines, Method B vs Method C

Technique and Criteria.

The general discussion of Methods B and C points out that the techniques are the same except that in Method B all significant layers were considered.

Figures 11-14 point out the differences in location of SS ridges caused by differences in SS values at individual stations where thin layers ($\lesssim$10mb) were present. Each analysis was accomplished without referring to charts produced by the alternate method, and therefore are as objective as possible.

Criteria for ridge location are the same as those discussed in Appendix I for Method A.

850-mb 00Z 20 August 1965. (Figure 11)

This chart illustrates how changes in two values (stations 327 and 451) can adjust the location of SS ridge lines by as much as 200 miles. The lower value of .000 calculated by Method B forces the ridge well north of station 327, and away from the NMC front through the area (Figure 15). The other ridges are identical, since no other thin layers were encountered.

700-mb 00Z 20 August 1965. (Figure 12)

Numerous thin layers at 700-mb force a Method B pattern which differs considerably from Method C and GGθ ridges as shown by Figure 16. As can be seen in that figure, Method C ridges have very high correlation with the FNWF numerical fronts, but Method B produces a wavy, random pattern

which does not correlate well with GGθ. It appears that the elimination of thin layers (Method C) has smoothed and adjusted Method B into a meaningful SS ridge analysis. Certainly this 700-mb chart seems to justify the arguments presented in section 4.

500-mb 00Z 20 August 1965. (Figure 13)

The 500-mb analysis shows, once again, how changes in SS values tend to alter the SS ridge lines. Since verification of both Methods B and C with FNWF's numerical fronts is fair to poor on this chart (see also Figure 17), comments will be limited to pointing out that Method C again seems to smooth out the ridge pattern, yielding a more meteorologically satisfying pattern.

300-mb 00Z 20 August 1965. (Figure 14)

Method C simply modifies a "no correlation" pattern to another "no correlation" pattern over central Canada. Only five values differ, and the pattern by both methods is subjective due to sparse data and a wide variation of values.

Derivation of Equation (5)

IF: $\theta = a + bp + cp^2$

$$\frac{\partial \theta}{\partial p} = b + 2cp$$

$$\theta_1 = a + bp_1 + cp_1^2$$

$$\theta_2 = a + bp_2 + cp_2^2$$

$$\theta_3 = a + bp_3 + cp_3^2$$

$$\theta_1 - \theta_2 = b(p_1 - p_2) + c(p_1^2 - p_2^2)$$

$$\theta_2 - \theta_3 = b(p_2 - p_3) + c(p_2^2 - p_3^2)$$

$$[(p_1 - p_2)(p_1 + p_2)]$$

$$(\theta_1 - \theta_2)p_2 - p_3 = b(p_1 - p_2)(p_2 - p_3) + c[(p_1^2 - p_2^2)(p_2 - p_3)]$$

$$(\theta_2 - \theta_3)p_1 - p_2 = b(p_1 - p_2)(p_2 - p_3) + c[(p_2^2 - p_3^2)(p_1 - p_2)]$$

$$*(\theta_1 - \theta_2)\Delta p_u - (\theta_2 - \theta_3)\Delta p_1 = c\left[(\Delta p_1)(p_1 + p_2)\Delta p_u - \{\Delta p_u(p_2 + p_3)\Delta p_1\}\right]$$

$$(\theta_1 - \theta_2)(p_2^2 - p_3^2) = b(p_1 - p_2)(p_2^2 - p_3^2)$$

$$(\theta_2 - \theta_3)(p_1^2 - p_2^2) = b(p_2 - p_3)(p_1^2 - p_2^2)$$

$$(\theta_1 - \theta_2)\Delta p_u(p_2 + p_3) - [(\theta_2 - \theta_3)\Delta p_1(p_1 + p_2) =$$

$$b[\{p_1\Delta p_u(p_2 + p_3)\} - \{\Delta p_u \Delta p_1(p_1 + p_2)\}]$$

RECALL: $\frac{\partial \theta}{\partial p} = b + 2cp$

$$\frac{\partial \theta}{\partial p} = \frac{\Delta\theta_1\Delta p_u(p_2 + p_3) - \{\Delta\theta_u\Delta p_1(p_1 + p_2)\}}{\Delta p_1\Delta p_u(p_2 + p_3) - \{\Delta p_u\Delta p_1(p_1 + p_2)\}} + 2p\frac{\{\Delta\theta_1\Delta p_u - \Delta\theta_u\Delta p_1\}}{[\Delta p_1\Delta p_u(p_1 + p_2 + \{\Delta p_u\Delta p_1(p_2 + p_3)\}]}$$

$$= \frac{\Delta\theta_1\Delta p_u(p_2 + p_3) - \Delta\theta_u\Delta p_1(p_1 + p_2)}{\Delta p_u\Delta p_1\Delta p} + 2p\frac{[\Delta\theta_1\Delta p_u - \Delta\theta_u\Delta p_1]}{-\Delta p_1\Delta p_u\Delta p}$$

$$= \frac{\Delta\theta_1(p_2 + p_3)}{\Delta p_1\Delta p} - \frac{\Delta\theta_u(p_1 + p_2)}{\Delta p_u\Delta p} - \frac{2p\Delta\theta_1}{\Delta p\Delta p_1} + \frac{2p\Delta\theta_u}{\Delta p\Delta p_u}$$

*$\Delta p_u = (p_2 - p_3)$; $\Delta p_1 = (p_1 - p_2)$; Same for θ.

SINCE $p = p_2$ for mandatory levels:

$$\left(\frac{\partial\theta}{\partial p}\right)_2 = \frac{1}{\Delta p}\left(\frac{p_2\Delta\theta_1 + p_2\Delta\theta_1 - 2p_2\Delta\theta_1}{\Delta p_1}\right) + \frac{1}{\Delta p}\left(\frac{2p_2\Delta\theta_u - p_1\Delta\theta_u - p_2\Delta\theta_u}{\Delta p_u}\right)$$

THUS: $$\left(\frac{\partial\theta}{\partial p}\right)_2 = \frac{1}{\Delta p}\left(\frac{(p_2 - p_2)\Delta\theta_1}{\Delta p_1} + \frac{(p_2 - p_1)\Delta\theta_u}{\Delta p_u}\right)$$

($-\Delta p_u$ over $(p_2 - p_2)$; $-\Delta p_1$ over $(p_2 - p_1)$)

As an example of this equality, consider station 520 Pittsburgh, Pennsylvania, at 850-mb.

PRESSURE	P.TEMPERATURE
883	298.6
850	300.1
771	301.8

Computer result, using parabolic fit, SS = .1082

By finite differencing:

$$\frac{\partial\theta}{\partial p} = \frac{1}{\Delta p}\left[\frac{\Delta p_u\Delta\theta_1}{\Delta p_1} + \frac{\Delta p_1\Delta\theta_u}{\Delta p_u}\right]$$

$$= \frac{1}{112}\left[\frac{19 \times 1.5}{33} + \frac{33 \times 1.7}{29}\right] = .0383$$

$$SS = \frac{p}{\theta}\frac{\partial\theta}{\partial p} = \frac{850}{300.1} \times .0383 = .1083$$

Error in fourth place.

APPENDIX III

SS Analysis by Method C

Comparison of SS with GGθ and NMC Fronts

Technique and Criteria.

SS computations by Method C were plotted and analyzed applying the principles discussed in SS Analysis by Method A. (Appendix I)

850-mb 00Z 20 August 1965. (Figure 15)

Four distinct SS ridge lines appear: (1) from just north of Newfoundland through New England south to West Virginia and west to Kansas; (2) from North Dakota across western Canada to the Pacific; (3) extreme northern Canada; and (4) western Alaska. The position of (1) seems well defined by a dense data network in its northeastern portion where the position is dictated by reports at only five stations: 816, 815, 807, 712, and 600. Since these five stations cover 250,000 square miles, location northeast of station 712 is questionable. The position at 712 looks very good, since a strong maximum occurs there at 700-mb, indicating that the 700-mb front is over the station and, therefore, the 850-mb front should be southeast of 712, as plotted. Along the eastern seaboard the ridge line lies within the .150 contour, and its western end is anchored by high readings at stations 456 and 451. This ridge verifies well with the NMC front, with differences of less than fifty miles along 50% of its route. The position of the ridge line seems to split the difference between the NMC front and the GGθ ridge. The ridge over western Canada is based on just a few readings, and would not have been drawn in except for the reading at station 867. It is interesting to note that the ridge line could have been drawn from station 945

north to the strong maximum over station 938. This points out the subjectivity inherent in hand analysis in sparse data areas. The ridge in northern Canada is based entirely on the enormous maximum over station 938. The ridge is well defined in the heart of a baroclinic zone. Lack of data prevented continuing this ridge farther east. Negative stability layers are found at several western stations. These negative values result from one significant layer showing $\gamma > \gamma_d$, a not uncommon occurrence over the desert areas in summer at 850-mb. It is also interesting to note high SS along the California coast. This is probably the trade-wind inversion (Figure 3) affecting stability at 850-mb. Finally, many readings in the Rocky Mountain area are missing because of altitude.

700-mb 00Z 20 August 1965. (Figure 16)

The pattern here shows four ridges. The ridge across the eastern United States is the same ridge which appeared on the 850-mb chart and shows excellent vertical consistency, in that it trails the 850-mb ridge by about 100 miles. If one considers the slope of a cold front to be about 1/100 between 850 and 700-mb, the ridge position looks reasonable. SS trails GGθ over the eastern one third of its path and the distance between the two ridges broadens to 150 miles over Missouri and Iowa, but northwest of South Dakota the two ridges are in very close proximity. The ridge in northeastern Canada is based on one large reading at station 090. This ridge could just as well have been omitted, since there are no hints as to orientation and direction. A ridge over the Pacific Northwest is well defined, but does not lie in a baroclinic zone, and does not have a counterpart at the 850- and 500-mb levels. A ridge across Alaska east and south into

central Canada compares fairly well with a GGθ ridge. The SS ridge is much longer on its southern end, however, based on high SS over stations 945 and 848. The vertical consistency of this ridge is not outstanding, but this could well be a function of the sparse data area. The western portion of this frontal structure which lies in a baroclinic zone, shows vertical consistency, but over central Canada there is no baroclinic zone, and the front meanders noticeably. A general feature of this chart is the flat gradient over the southeast, south central, and Rocky Mountain states. SS is not high except over station 304, and since SS increases to the north, no ridge was drawn even though the 500-mb analysis shows a ridge in the vicinity.

500-mb 00Z 20 August 1965. (Figure 17)

The ridge pattern at 500-mb shows four ridges. The 500-mb ridge over the eastern United States shows high positive correlation with GGθ and with the SS ridge at 850 and 700-mb from Newfoundland to Ohio. Northwest of Ohio SS moves steadily away from GGθ, taking a more northerly route out of the baroclinic zone. It may well be that the SS ridge does follow GGθ and maintains vertical continuity with the ridges at lower levels, but high readings over stations 747 and 645, plus low readings at 945 and 879, make it difficult to draw a ridge across southwestern Canada. A well defined ridge over the southern states is not considered frontal, since it is not vertically consistent with a lower level front and does not lie in a baroclinic zone. The same comments can be made about a ridge from Colorado to Washington. However, the ridge over Alaska into Canada is vertically

consistent with ridges mentioned at lower levels, and lies in a baroclinic zone. Whether this ridge actually ties into the ridge over the midwestern United States is conjecture. It is not surprising that certain difficulties are encountered at 500-mb. Some cold fronts may not extend to this altitude, or the character of the front may change. As pointed out by Gates, the value of static stability may begin to reduce at this level, a fact which may affect the pattern.

300-mb 00Z 20 August 1965. (Figure 18)

This chart appears to be of little value in location of ridge lines which represent fronts. It does seem that SS values are lower at this level, as evidenced by the extensive flat gradient over the entire United States, with average values of .060. There are three definable ridge lines on the chart, but none are associated with lower level ridges and only the one over the desert southwest lies in a baroclinic zone.

It seems logical that fronts, if they exist at all, will be hard to find at 300-mb. Since data are sometimes taken up to 250-mb, some of the higher stability values may be caused by the tropopause instead of by frontal layers. Thus the value of this particular system at 300-mb is questionable. For example, analysis of the soundings for stations 906, 909, and 913 show the tropopause between 250 and 300-mb. This stable zone gives high values of SS and a false indication of a frontal zone.

850-mb 1200Z 20 August 1965. (Figure 20)

The major ridge along the eastern seaboard shows time continuity in that it has progressed at 15 knots over the eastern states and 25 knots over the southern states. The ridge remains very close to the NMC front through

the area, with a maximum separation of 100 miles near Cape Hatteras. The GGθ ridge also correlates well, except over Newfoundland and a questionable area over the southeastern states. In this area, GGθ turns north as the baroclinic zone separates into two branches. The SS ridge continues across northern Texas, then northwest into the Pacific, anchored by a series of very high readings across the western United States. Another secondary ridge, also in a baroclinic zone, extends from Delaware west to South Dakota. This matches well with GGθ, but has only a small NMC counterpart over South Dakota and has no time continuity with any ridge on the 00Z chart. This ridge could be the result of a subsidence inversion in the cool air behind the front. The ridge over Alaska and northwest Canada is essentially stationary from 00Z, and still lies in a baroclinic zone. This ridge is more extensive than at 00Z, however. A new ridge over extreme northern Canada appears very strong, but there is no baroclinic zone in the area.

An interesting feature of this chart is a large mass of air with low stability which dominates central Canada. This mass will be found to persist at all levels, and seems to be a feature of the atmosphere behind an advancing cold front.

700-mb 1200Z 20 August 1965. (Figure 21)

The ridge line along the eastern seaboard compares very closely with GGθ over its entire path from southeast Canada to Montana, but west of Delaware it is closely related to the ridge at 850-mb which was considered the secondary ridge. The ridge across the southern states which was strong at 850-mb is still strong at 700-mb, but is not continuous across North

Carolina and Virginia. Considering the high reading at station 317, a higher reading at station 402 would have allowed a ridge to intersect the strong ridge near station 506, an event which would have given outstanding correlation with the SS ridge as shown at 850-mb. The ridge over extreme northern Canada has vertical continuity with the 850-mb ridge, but still does not lie in a baroclinic zone. The ridge over northwest Canada and Alaska looks very realistic over its western portion, but the eastern half is questionable because of a lack of data.

500-mb 1200Z 20 August 1965. (Figure 22)

The ridge across the northern United States is well defined and has consistency with its GGθ counterpart. It also remains imbedded in the baroclinic zone. The ridge over the southeast is not in a baroclinic zone, and appears to be non-frontal. The ridge over the southwest desert is in a baroclinic zone and compares well with GGθ in the area. The ridge over Alaska and northwest Canada is still stationary over its western portion, but enters a strong north-south baroclinic zone over western Canada, and lies very close to the GGθ ridge in the area. Another short ridge over central Canada is based on two readings and appears non-frontal.

Again at 500-mb a large area of low stability exists over eastern Canada behind the ridge.

300-mb 1200Z 20 August 1965. (Figure 23)

The chart is characterized by small SS over the entire United States with the exception of two readings of .15 at stations 583 and 576 which define a short ridge over the Nevada, Idaho, Wyoming area. Higher values exist over Canada, with a ridge stretching from the Great Lakes north, but

the tropopause is responsible for high values of SS at stations 109, 722, and 943. There is little data to support placing this ridge entirely inside the baroclinic zone outlined by GGθ, but contours of SS are generally parallel to the ridge and trough lines of GGθ. As indicated in the discussion of SS at 300-mb for 00Z, there appears little resemblance between the pattern at this level and those below.

APPENDIX IV

SS Analysis by Method C

Comparison of SS with the FNWF Static Stability (σ) Analysis

Technique and Criteria

FNWF's hemispheric printout of σ for 00Z 20 August 1965 displays areas of positive and negative σ (relative to standard reference values) [6]. In some cases these areas are large, with a noticeable gradient, while in other cases small pockets of positive or negative values show up.

The printouts for the lower four layers were analyzed for ridge lines of σ. This analysis was somewhat subjective since no specific guide lines were available. Whenever possible, positive areas were connected by a ridge line, even though a small area of negative values separates the positive areas. When a small positive pocket was completely surrounded by negative values, no ridge was drawn. The ridge lines themselves were smoothed (i.e., avoiding kinks and sharp corners), whenever feasible, in order to present a more reasonable analysis. No distinction was made between a narrow, well defined, positive zone and a wide, poorly defined one. No difference was noted between low positive and high positive values either, as long as they represented relative maxima.

These ridge lines were transferred to Figures 15-18 and compared with SS ridges.

850 mb 00Z 20 August 1965. (Figure 15)

SS at 850-mb is compared with the FNWF σ for the layer 1000-775-mb. FNWF's σ is a meandering ridge line, which moves in and out of the baroclinic zone. If one assumes that the GGθ ridge and the NMC front are

properly located, then σ is a rather poor representation of a frontal zone, especially over the middle west. The SS ridge, on the other hand, is smoother, comparing closely with GGθ and NMC and lying almost entirely within the baroclinic zone. SS and σ have a close comparison only over the middle Atlantic states. One factor tending to produce these variations is that σ considers the atmospheric structure near the surface -- that is, near 1000-mb. Thus, the static stability picture may be confused by layers of air near the surface which represent local terrain features. For example, the wide swing of σ out over the Atlantic Ocean may have been caused by relatively stable air over the ocean east of Boston -- a not uncommon weather feature in summer. On the other hand, SS is computed for the layers around 850-mb, and this altitude may be above low level inversions. The other two σ ridges over the western United States and northern Canada compare poorly with GGθ and SS.

700-mb 00Z 20 August 1965. (Figure 16)

Considering the ridges over the eastern United States, SS and σ parallel each other with SS generally 120 miles on the warm air side of σ.

The σ ridge over central and western Canada is in an area of low SS and does not compare well, except over northwestern Canada and Alaska. The two small σ ridges over the southeast United States and eastern Canada are not verified with GGθ or SS ridges.

500-mb 00Z 20 August 1965. (Figure 17)

At this level both ridges have less correlation with the GGθ ridge and the baroclinic zones than in lower layers, but σ is particularly poor, with only about 25% lying in a baroclinic zone and almost no σ ridge to

compare with GGθ. There are at least two locations on the chart where ridges cross GGθ ridges at right angles. σ does have a slightly better positive correlation with SS, possibly because the two quantities have some similarities.

300-mb 00Z 20 August 1965. (Figure 18)

Neither σ nor SS ridges can justifiably be called good representations of frontal phenomena at this level, on the basis of this chart. As stated elsehwere in this project, neither ridge seems to give any meaningful information at 300-mb.

850-mb 1200Z 20 August 1965. (Figure 20)

The σ ridge over the northeastern United States parallels SS and GGθ ridges, generally about 100 miles on the warm side of both. However, over the middle western states the σ ridge is weak and shows poor comparison with extensive GGθ and SS ridges in the same general area.

The σ ridges over the far western states and western Canada cross the SS ridges at right angles in at least two areas, and there is little basis for comparison. The same is true of the ridge over northern Canada when compared with GGθ and SS ridges over Alaska.

700-mb 1200Z 20 August 1965. (Figure 21)

The highest correlation between σ and SS exists at this level. This is a repeat of the situation which existed at 00Z. The σ ridge meanders across the SS ridge, while crossing the United States, but generally remains within 100 miles of the SS ridge.

The σ ridge over southwestern Canada is relatively weak and has no correlation with a SS ridge except over Alaska.

500-mb 1200Z 20 August 1965. (Figure 22)

At this level σ and SS ridges compare well over the northeastern United States, but the only other areas where comparison is possible are over Alaska, a small area over California, and over the central United States. In each case, the σ ridge leads the SS ridge, about 100 miles on the warm side of the SS ridge.

300-mb 1200Z 20 August 1965. (Figure 23)

The major σ ridge at this level compares fairly well with the SS ridge, and very well with the GGθ ridge over Canada.

The analysis over the western states has no SS ridges with which to compare the σ ridges. The two σ ridges are weak, however, and their existence is somewhat subjective.

Appendix IV pointed out the dominance of low values of SS at 300-mb, and the σ printout is also dominated by low values, the majority of which are negative. Both of these findings agree with the conclusions of Gates, who found lower values of static stability above 500-mb [3].

APPENDIX V

$\Delta G\theta$

Comparison of computed $G\theta$ using significant level data with FNWF's $G\theta$ using processed data. $\Delta G\theta$ values are determined using computed $G\theta$ as base.

850-mb: 86 Stations Computed

$\Delta G\theta$ = computed $G(\theta)$ − FNWF $G(\theta)$	All Stations	Stations within Baroclinic zone[7]	Stations outside Baroclinic zone[7]
+1.0	0	0	0
+.81 to 1.0	4	4	0
+.61 to .8	2	2	0
+.41 to .6	1	0	1
+.21 to .4	6	3	3
-.2	31	11	20
-.21 to -.4	8	2	6
-.41 to -.6	5	0	5
-.61 to -.8	7	0	7
-.81 to -1.0	6	0	6
-1.0	16	0	16
Average absolute difference	.50°	.33°	.56°
Median	-.34°	+.28°	-.52°

[7]The baroclinic zone has been arbitrarily defined as the zone bounded by the 1.0°C/100 km. isoline on computed $G\theta$ charts.

700-mb: 91 Stations Computed

$G\theta$ = computed $G(\theta)$ − FNWF $G(\theta)$	All Stations	Stations within Baroclinic zone[7]	Stations outside Baroclinic zone[7]
>+1.0	7	6	1
+.81 to 1.0	1	1	0
+.61 to .8	6	5	1
+.41 to .6	0	0	0
+.21 to .4	3	3	0
±.2	46	14	32
-.21 to -.4	15	0	15
-.41 to -.6	4	0	4
-.61 to -.8	5	0	5
-.81 to -1.0	1	0	1
<-1.0	3	0	3
Average absolute difference	.36°	.59°	.26°
Median	-.01°	+.59°	-.28°

FIGURE 1

GGθ (1000-700MB) 12Z 23 OCT 1965
— GGθ CONTOURS

FIGURE 2

SEA LEVEL PRESSURE & GGO ANALYSIS 23 OCT 1965

— GGO RIDGE

— PRESSURE CONTOURS

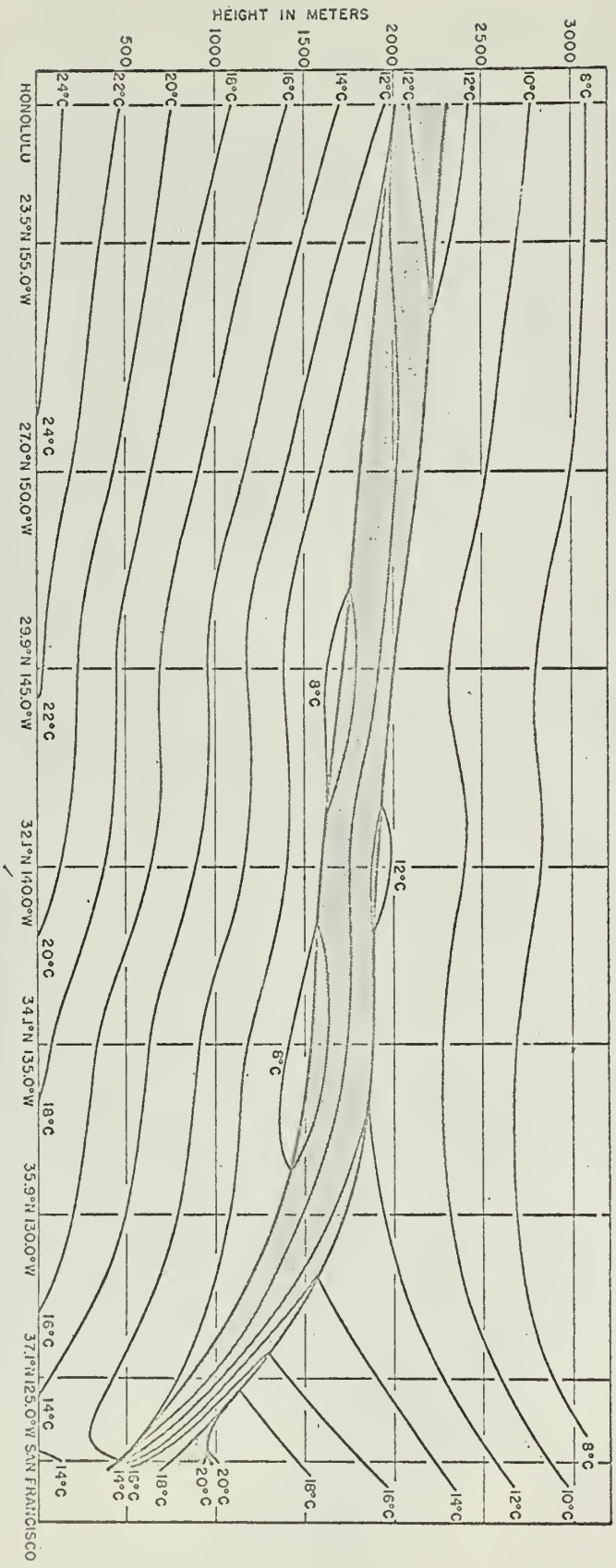
HEIGHT IN METERS
500
1000
1500
2000
2500
3000
HONOLULU 23.5°N 155.0°W
27.0°N 150.0°W
29.9°N 145.0°W
32.1°N 140.0°W
34.1°N 135.0°W
35.9°N 130.0°W
37.1°N 125.0°W SAN FRANCISCO
24°C
22°C
20°C
18°C
16°C
14°C
12°C
10°C
8°C

Figure 3

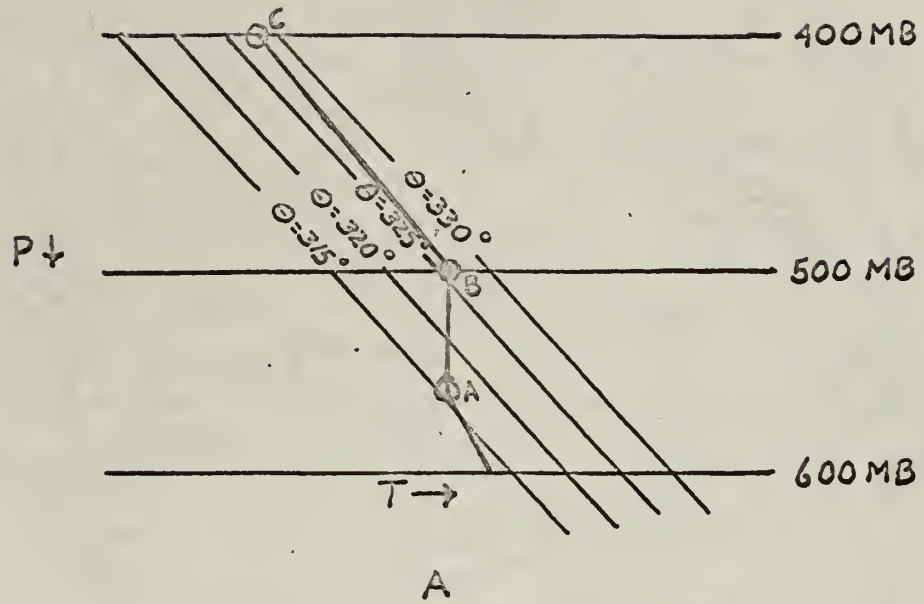
400 MB
500 MB
600 MB
P↓
T→
θ=330°
θ=325°
θ=320°
θ=315°
C
B
A

A

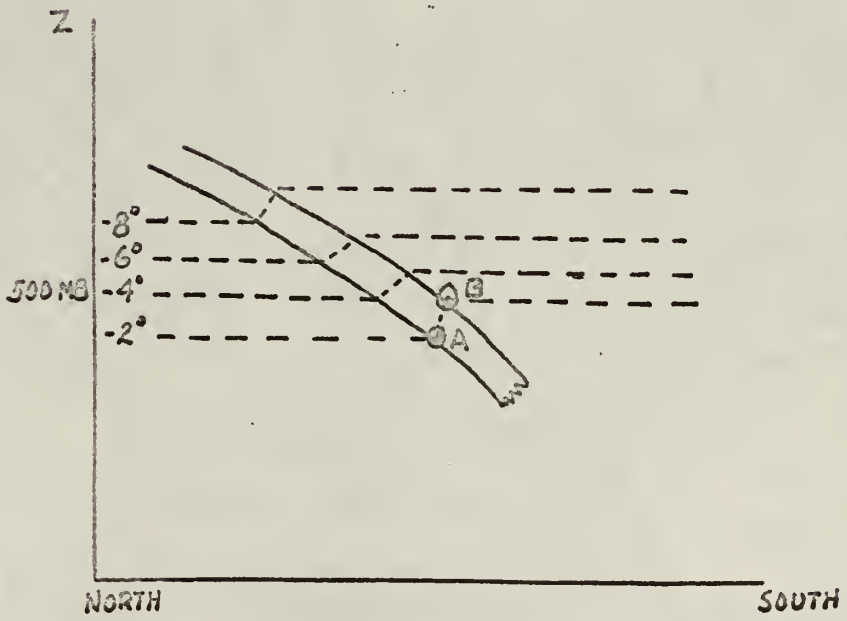
Z
-8°
-6°
-4°
-2°
500 MB
B
A
NORTH
SOUTH

B

Figure 4

Figure 5

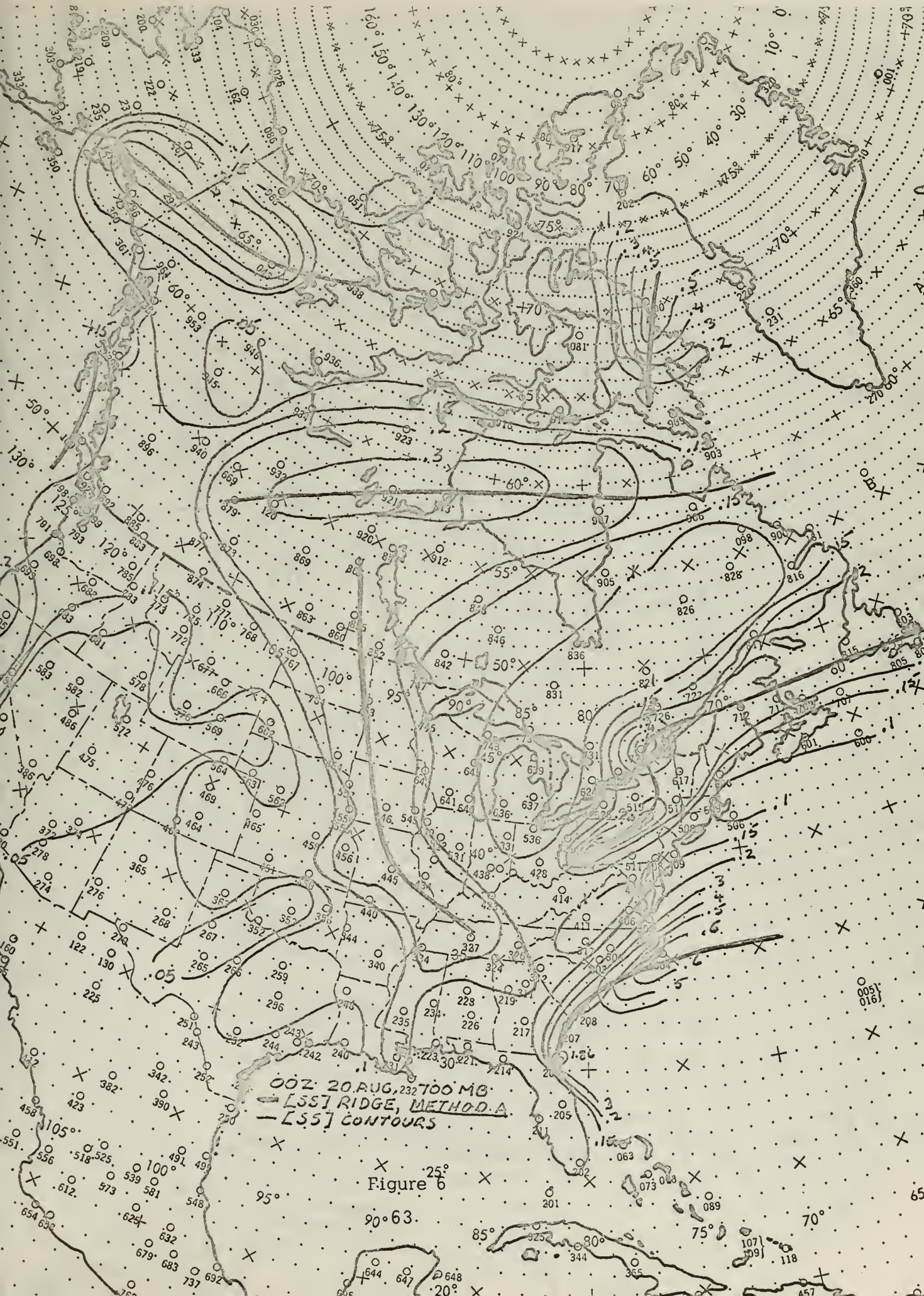

Figure 6

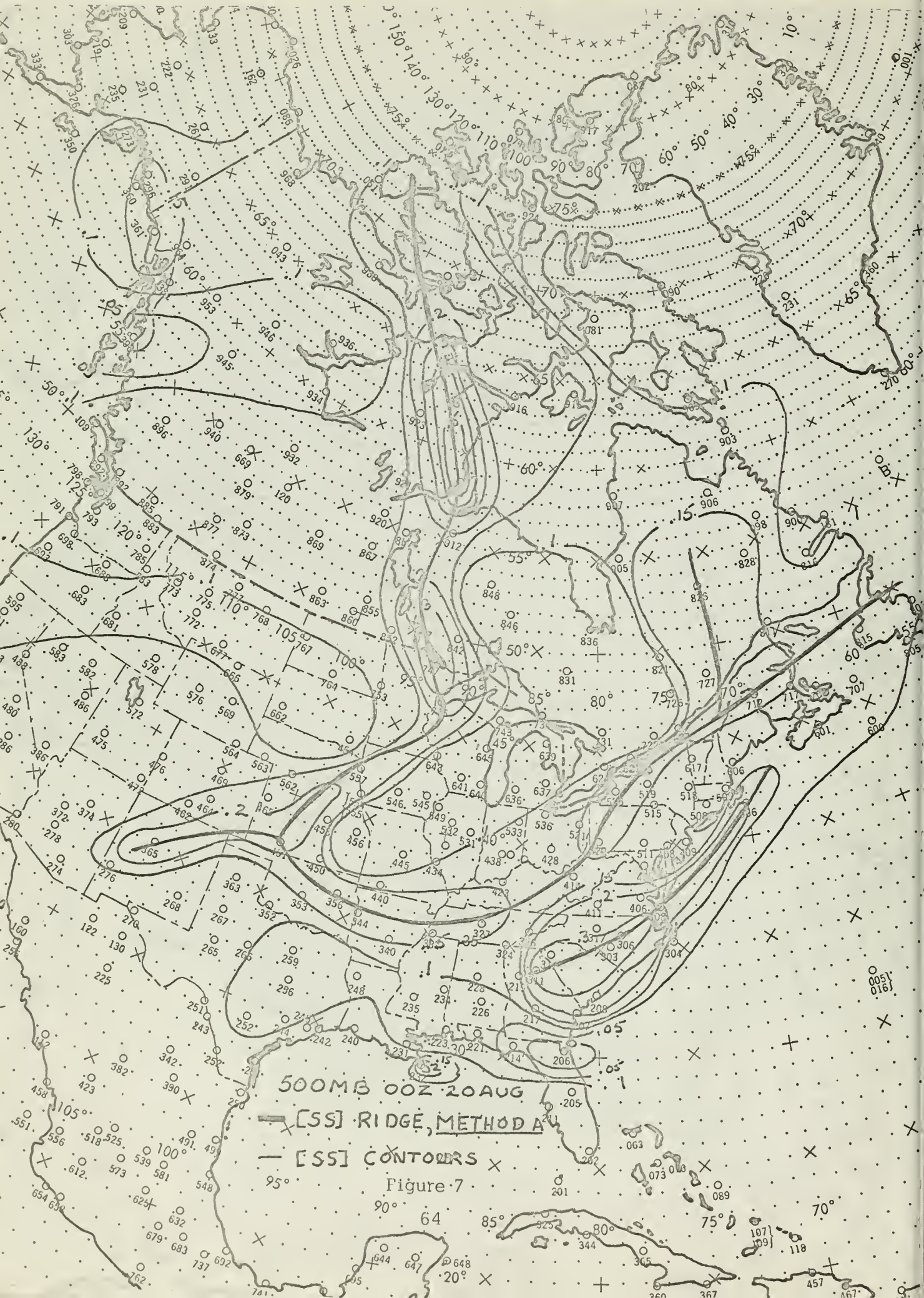

Figure 7

Figure 8

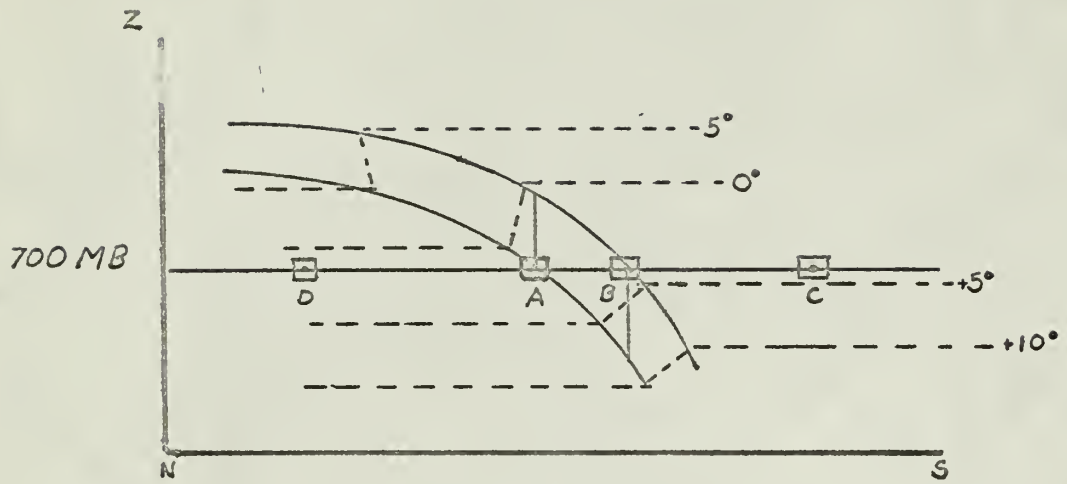

(A)

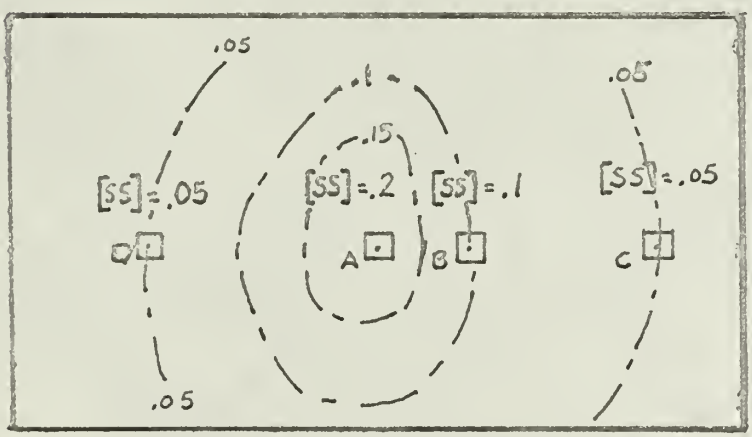

(B)

Figure 9

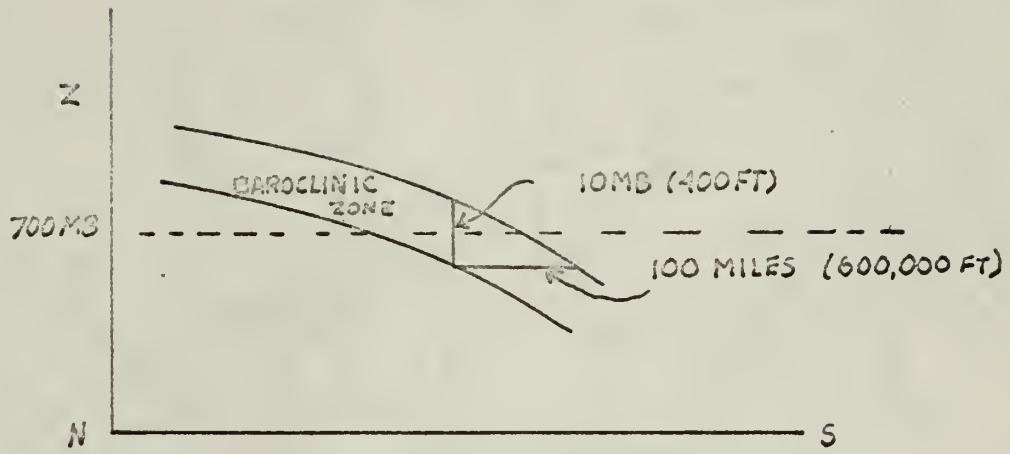

$$\text{SLOPE} = \frac{400}{600{,}000} = \frac{1}{1500}$$

Figure 10

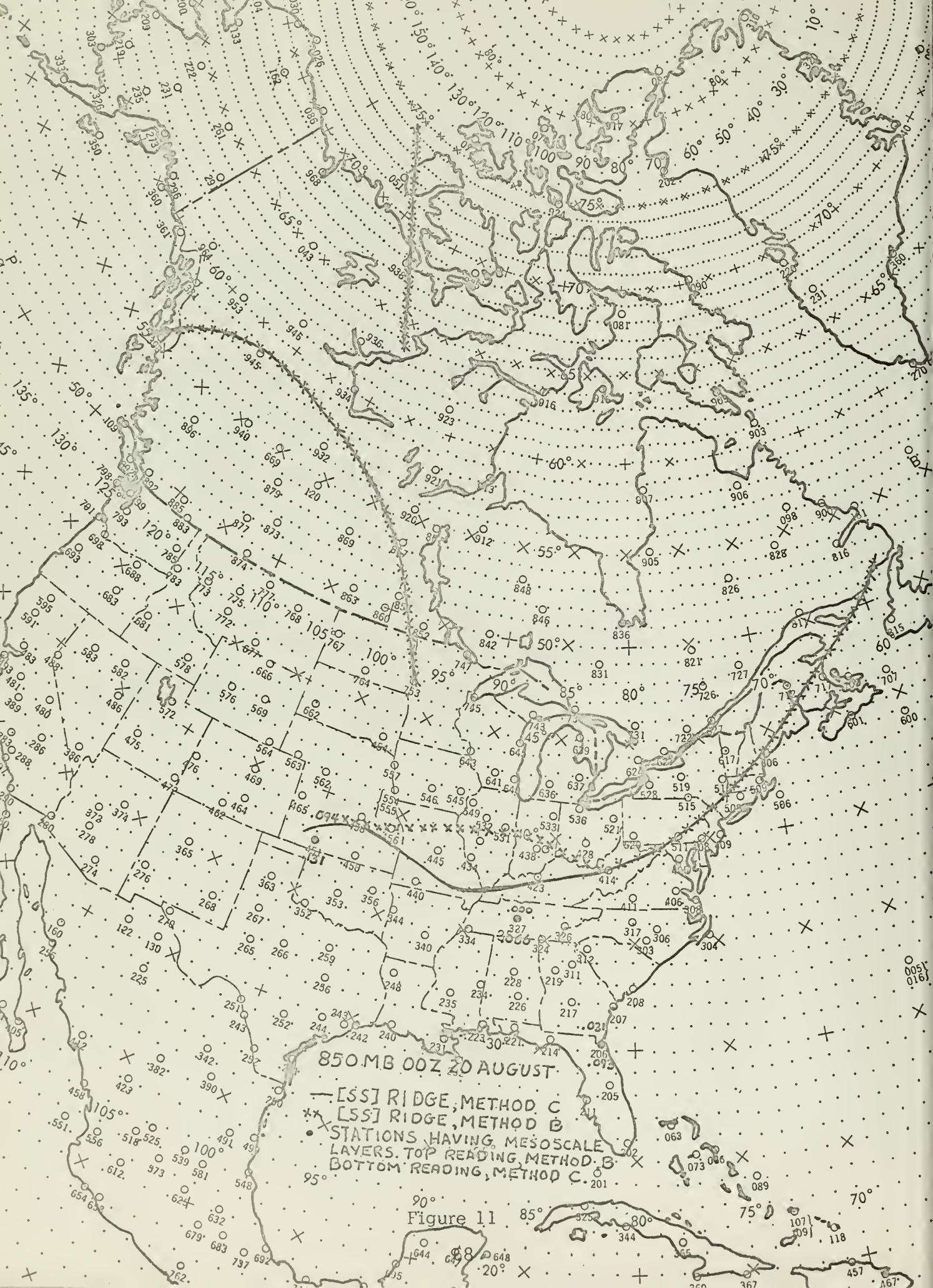
850 MB 00Z 20 AUGUST
[SS] RIDGE, METHOD C
[SS] RIDGE, METHOD B
STATIONS HAVING MESOSCALE LAYERS. TOP READING, METHOD B BOTTOM READING, METHOD C.

Figure 11

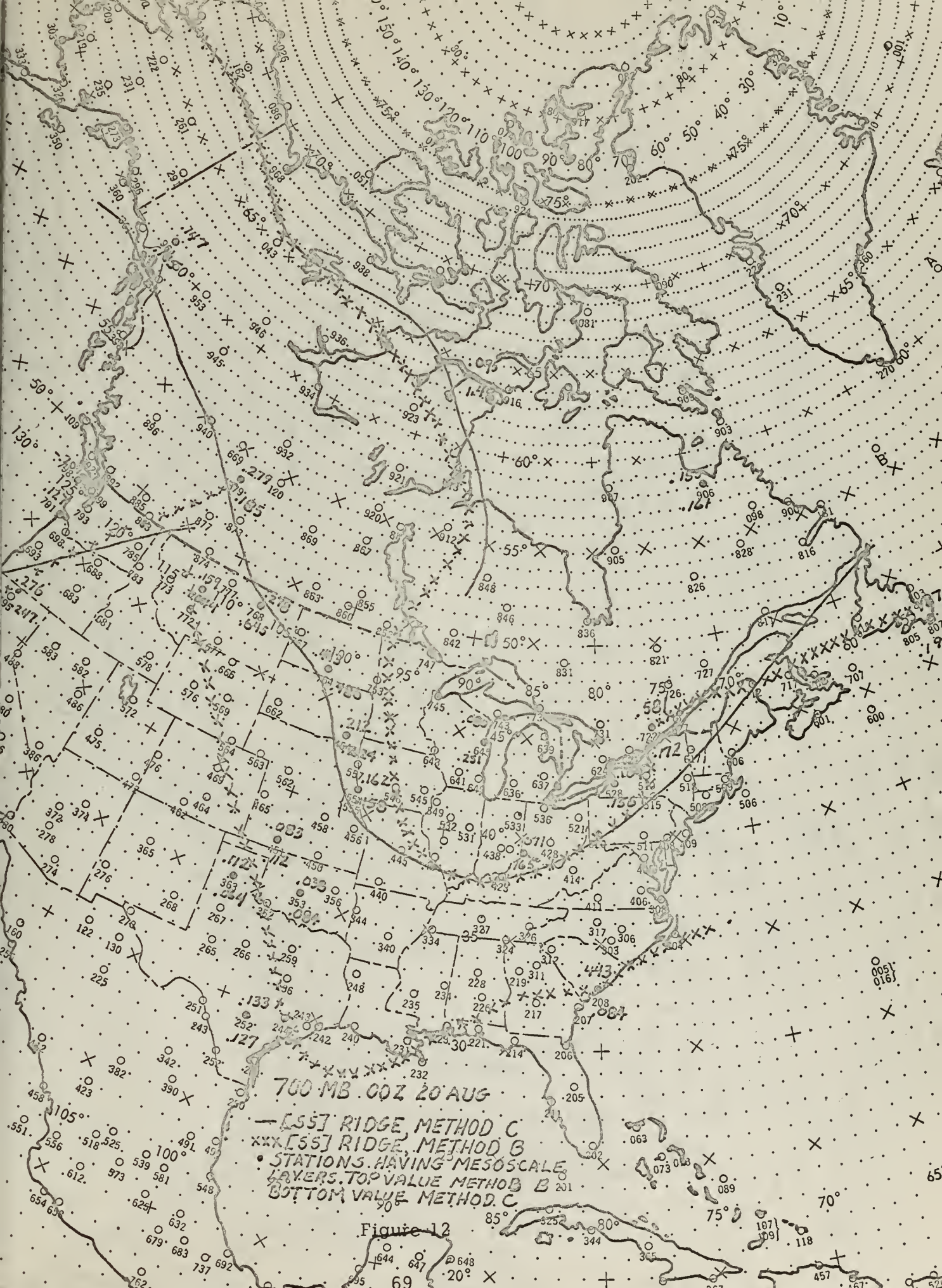
700 MB 00Z 20 AUG
—[SSS] RIDGE METHOD C
×××[SSS] RIDGE METHOD B
• STATIONS HAVING MESOSCALE LAYERS. TOP VALUE METHOD B BOTTOM VALUE METHOD C

Figure 12

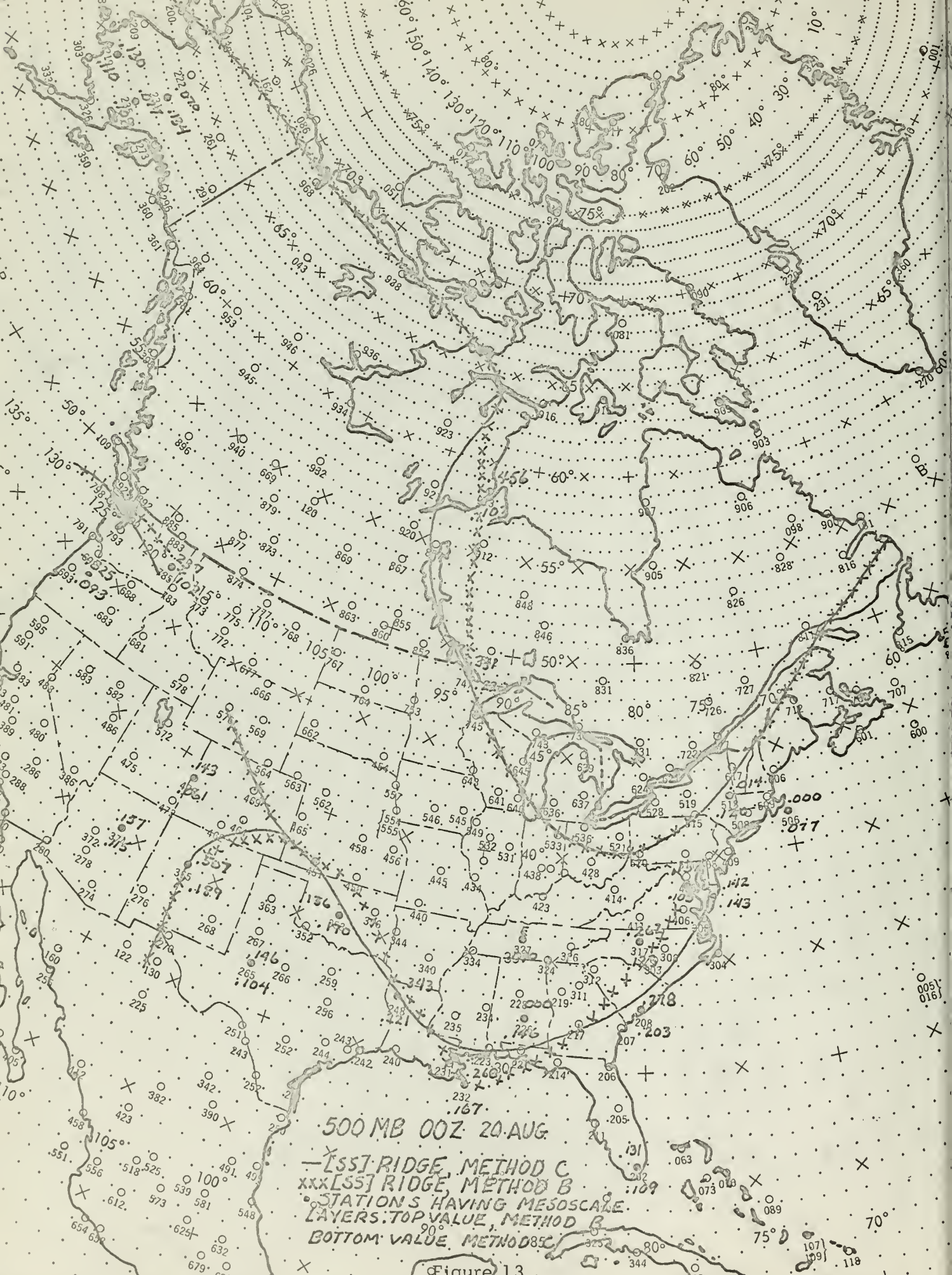
500 MB 00Z 20 AUG
—[SS] RIDGE, METHOD C
xxx[SS] RIDGE, METHOD B
STATIONS HAVING MESOSCALE
LAYERS: TOP VALUE, METHOD B
BOTTOM VALUE, METHOD C

Figure 13

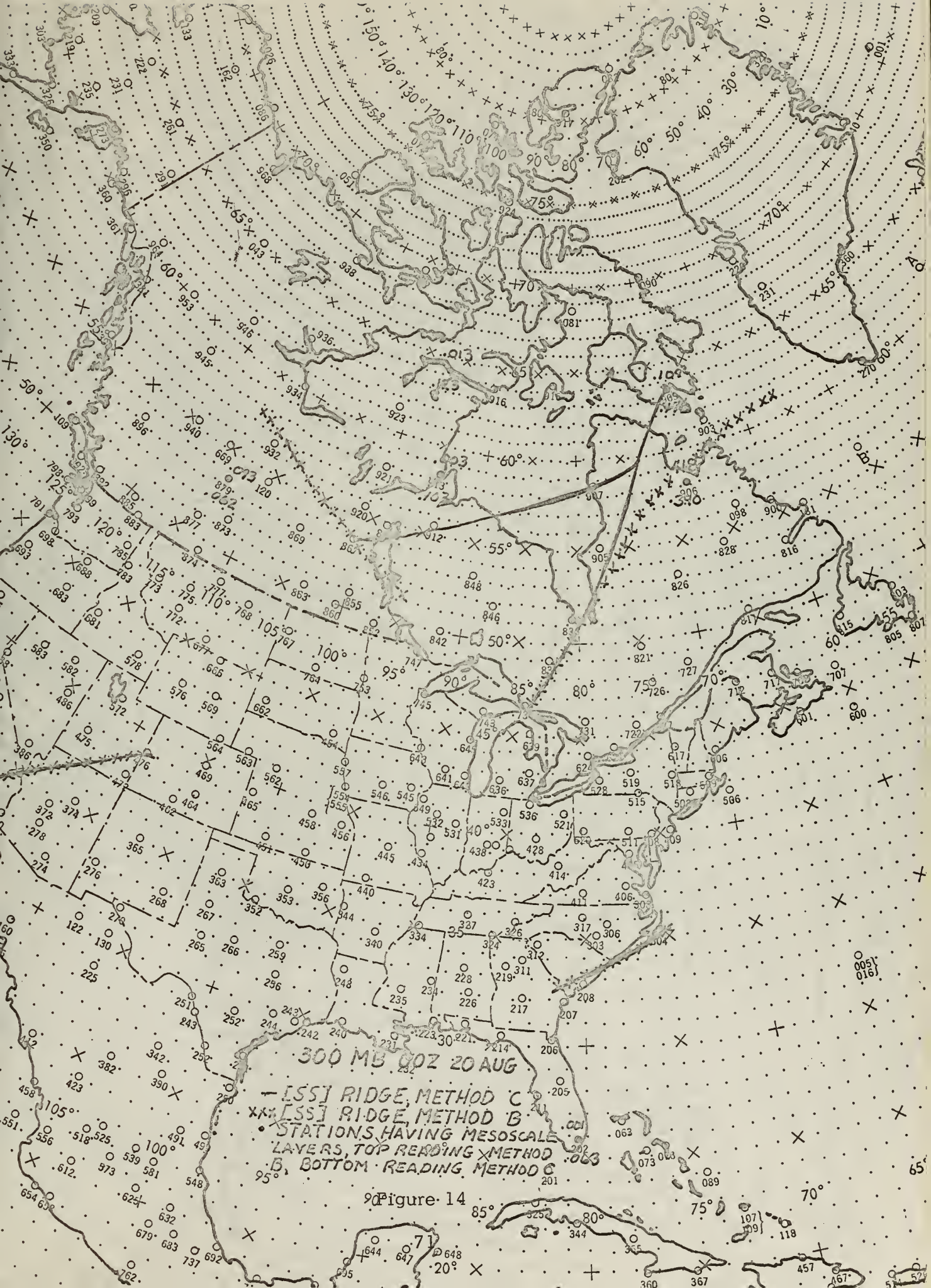
300 MB 00Z 20 AUG
[SS] RIDGE, METHOD C
[SS] RIDGE, METHOD B
STATIONS HAVING MESOSCALE
LAYERS, TOP READING METHOD
B, BOTTOM READING METHOD C

Figure 14


850 MB 00Z 20 AUG
[SS] RIDGE, METHOD C
NMC FRONT
XXX FNWF G, LAYER 1000-775 MB
95 GGO RIDGE (WARM BOUNDARY, B.Z.)
GGO TROUGH (COLD BOUNDARY, B.Z.)
[SS] CONTOURS

Figure 1-5


700 MB 082 20 AUG.
[SSS] RIDGE, METHOD 2
XXX FNWF G, LAYER 775-600
000 GGG RIDGE, WARM BOUNDARY OF
000 GGG TROUGH, COLD BOUNDARY OF
[SSS] CONTOURS

Figure 16

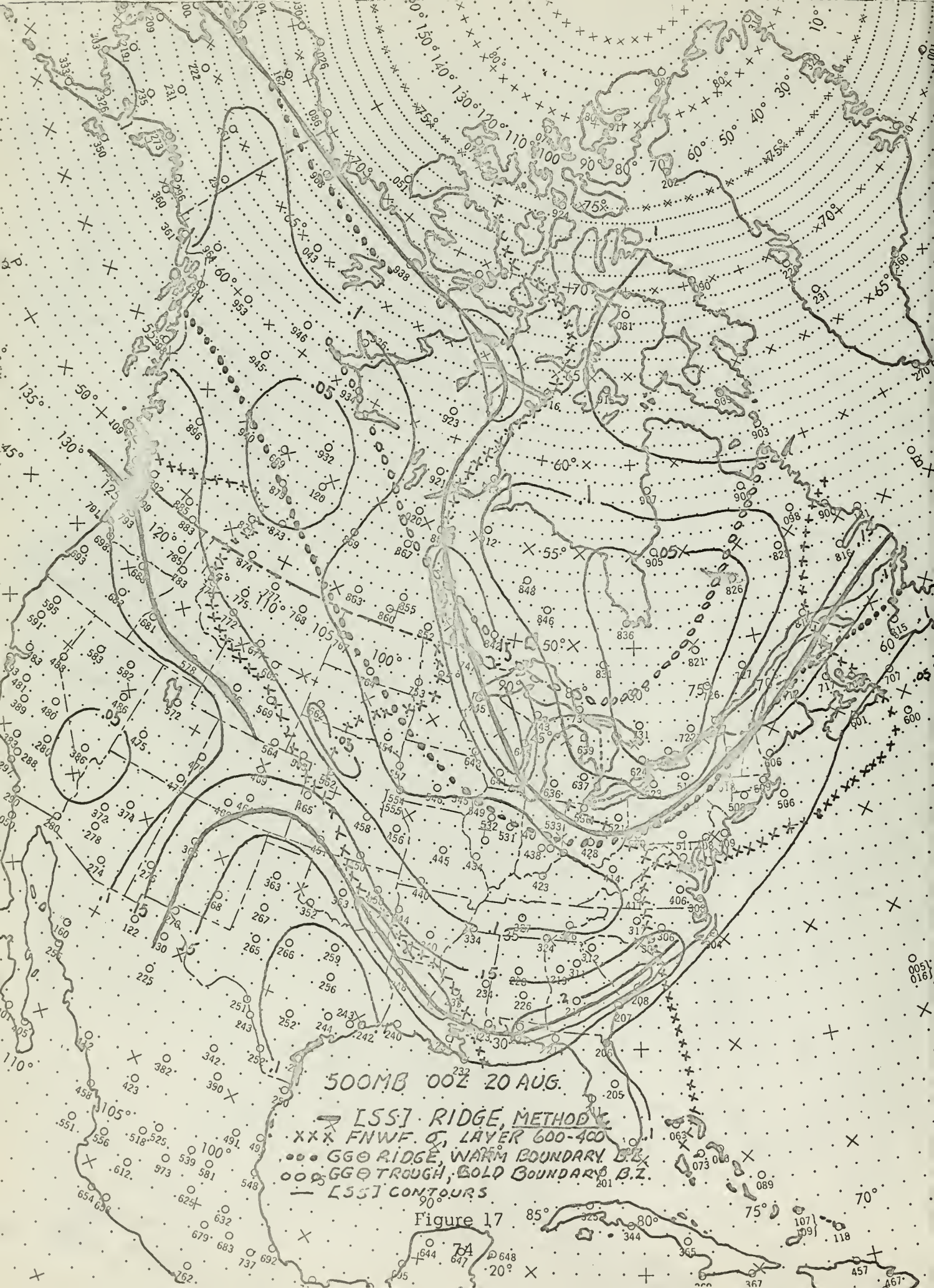
500MB 00Z 20 AUG.
[555] RIDGE, METHOD 1
XXX FNWF Q, LAYER 600-400
GGG RIDGE, WARM BOUNDARY B.Z.
GGG TROUGH, COLD BOUNDARY B.Z.
[555] CONTOURS

Figure 17

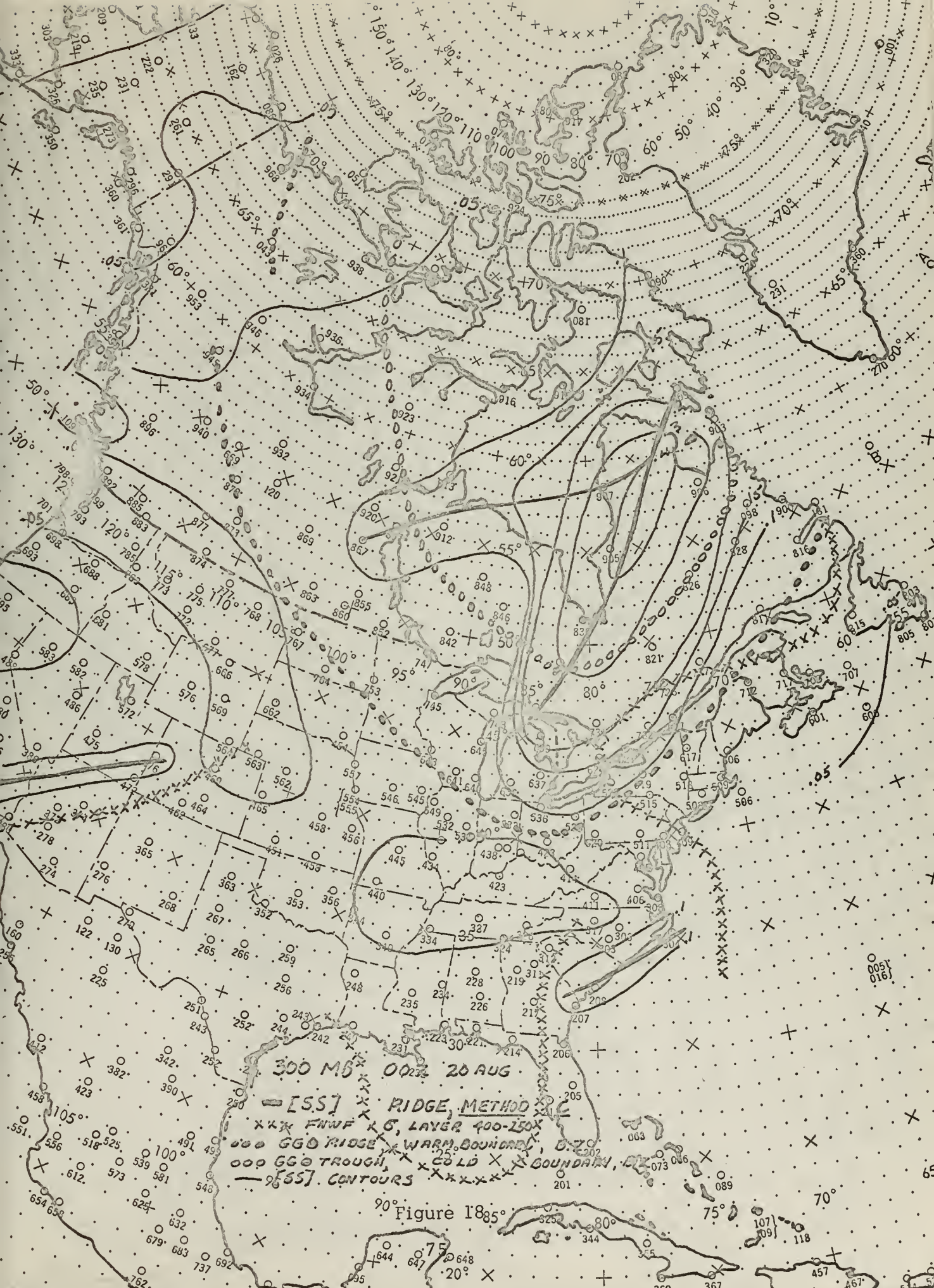
300 MB 00Z 20 AUG
[SS] RIDGE, METHOD C
FNWF C, LAYER 400-250
GGO RIDGE, WARM BOUNDARY, D-Z
GGO TROUGH, COLD BOUNDARY, D-Z
[SS] CONTOURS

Figure 18

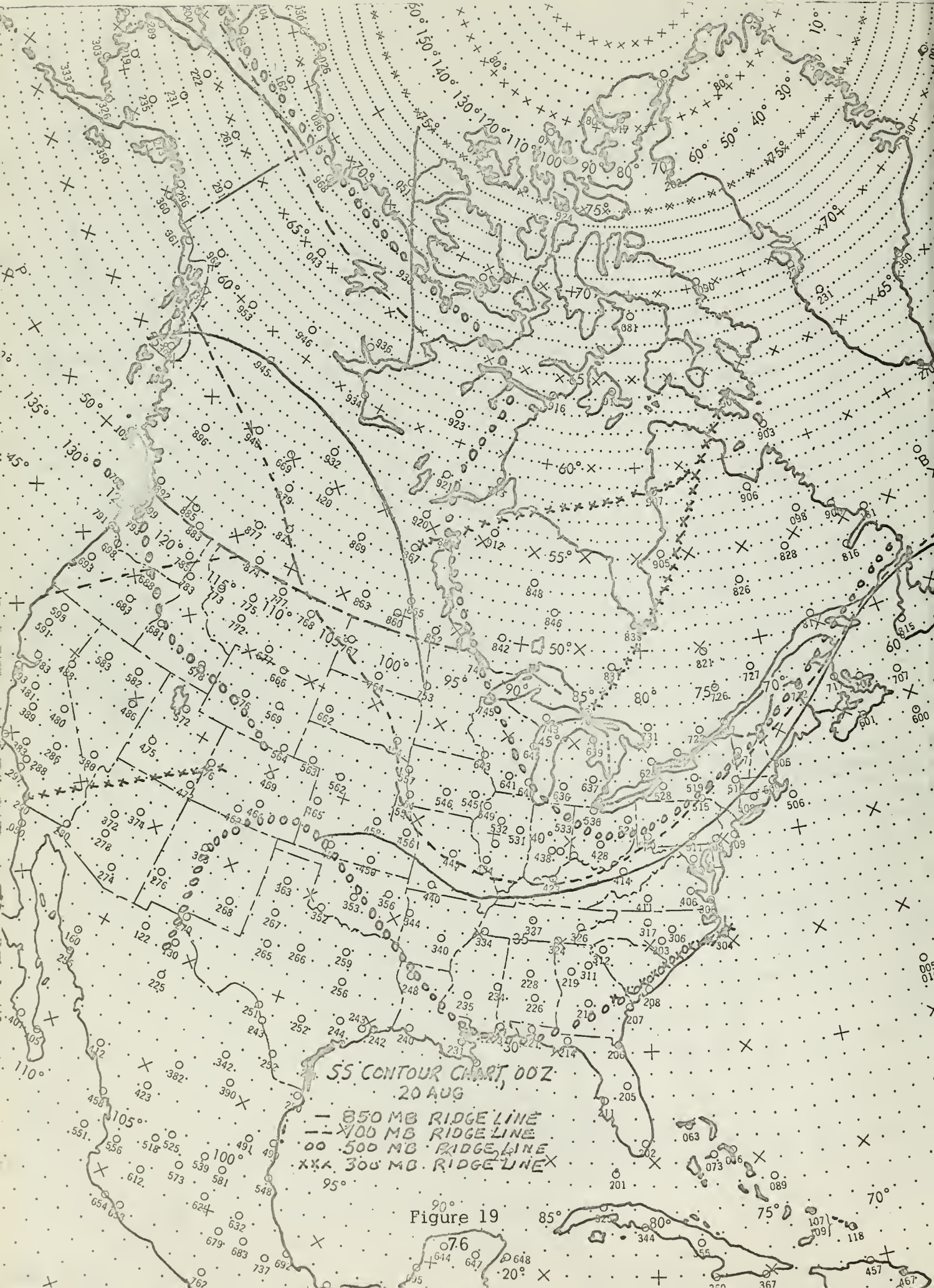
SS CONTOUR CHART, 00Z
20 AUG
— 850 MB RIDGE LINE
— — 700 MB RIDGE LINE
oo 500 MB RIDGE LINE
xxx 300 MB RIDGE LINE

Figure 19


850MB 12Z 20AUG.
[SSS] RIDGE, METHOD 0
NMC FRONT
XXX NWS 0 LAYER 1000-775
000 GGG RIDGE, WARM BOUNDARY BZ.
000 GGG TROUGH, COLD BOUNDARY BZ.
[SSS] CONTOURS

Figure 20

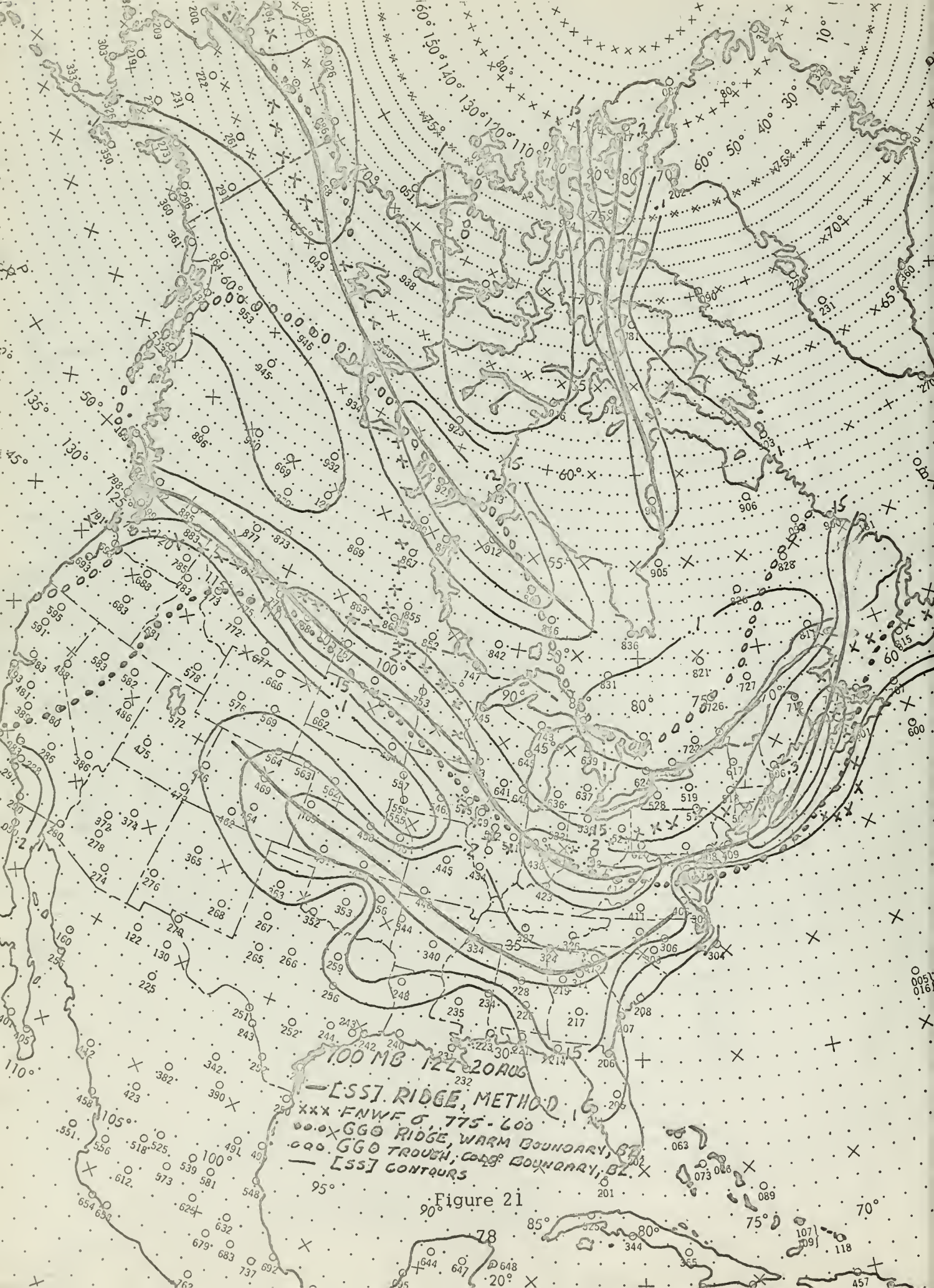
700 MB 12Z 20AUG
[SST] RIDGE, METHOD 1
XXX FNWF 6, 775-605
000 GGO RIDGE, WARM BOUNDARY, BZ
000 GGO TROUGH, COLD BOUNDARY, BZ
— [SST] CONTOURS

Figure 21

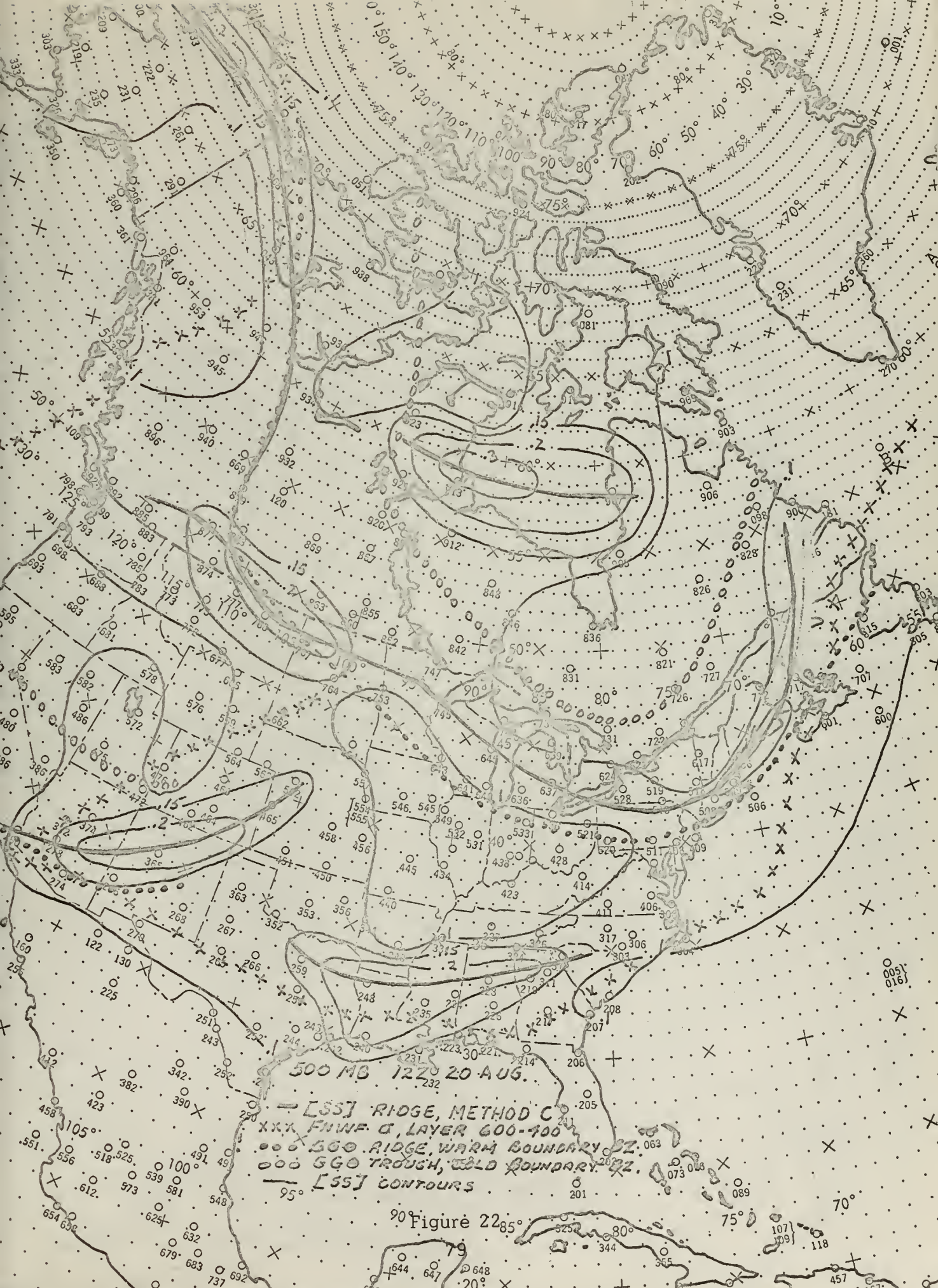
500 MB 122° 20 AUG.
— [SS] RIDGE, METHOD C
xxx FNWF C, LAYER 600-400
●●● GGO RIDGE, WARM BOUNDARY
○○○ GGO TROUGH, COLD BOUNDARY
— [SS] CONTOURS

Figure 22

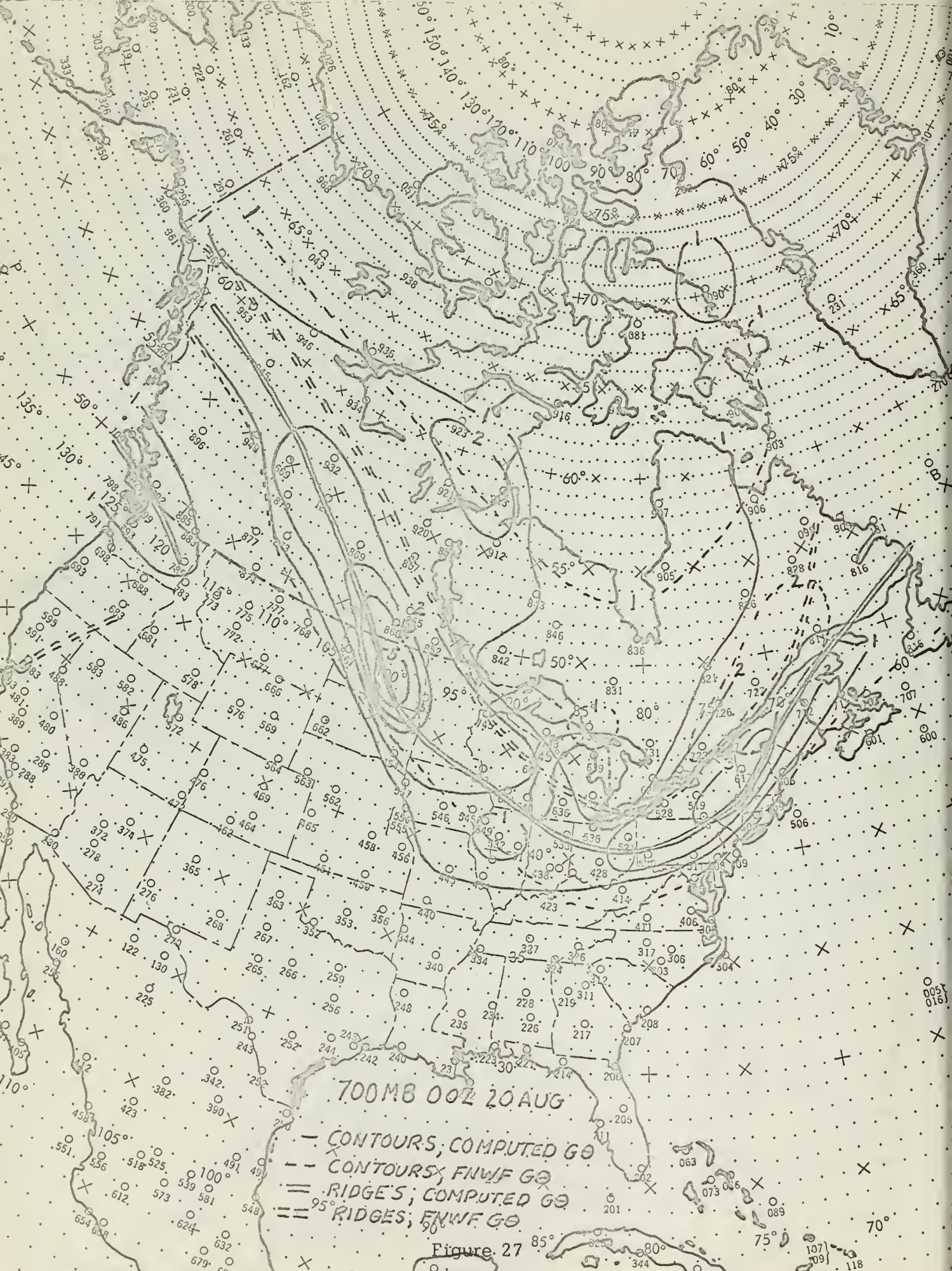
700MB 00Z 20AUG
— CONTOURS; COMPUTED GO
– – CONTOURS; FNWF GO
═ RIDGES; COMPUTED GO
═ RIDGES; FNWF GO

Figure 27

REVISED DISTRIBUTION LIST

Main Library, USNPG Sch	~~8~~ 12
Author	3
Advisor	2
Dept of Met. and Ocg., USNPG Sch	2
USN FNWF	2
Extra for future distribution (Dept of Met and Ocg.)	~~18~~ 19

4.	Officer in Charge Naval Weather Research Facility U. S. Naval Air Station, Bldg R-48 Norfolk, Virginia 23511	1
5.	Commanding Officer FWC/JTWC COMNAVMAR FPO San Francisco, Calif. 96630	1
6.	Commanding Officer U. S. Fleet Weather Central FPO Seattle, Washington 98790	1
7.	Commanding Officer U. S. Fleet Weather Central FPO San Francisco, California 96610	1
8.	Commanding Officer U. S. Fleet Weather Central FPO, New York, New York 09540	1
9.	Commanding Officer Fleet Weather Central Navy Department Washington, D. C. 20390	1
10.	Commanding Officer Fleet Weather Central U. S. Naval Air Station Alameda, California 94501	1

INITIAL DISTRIBUTION LIST (cont'd)

		No. Copies
11.	Commanding Officer and Director Navy Electronics Laboratory Attn: Code 2230 San Diego, California 92152	1
12.	Officer in Charge Fleet Numerical Weather Facility U. S. Naval Postgraduate School Monterey, California 93940	1
13.	U. S. Naval War College Newport, Rhode Island 02844	1
14.	Director, Naval Research Laboratory Attn: Tech. Services Info. Officer Washington, D. C. 20390	1
15.	Office of Chief Signal Officer Research and Development Division Department of the Army Washington, D. C.	1
16.	Commander Air Force Cambridge Research Center Attn: CROOTR Bedford, Massachusetts	1
17.	Geophysics Research Directorate Air Force Cambridge Research Center Cambridge, Massachusetts	1
18.	Mr. Leo Clarke Fleet Numerical Weather Facility U. S. Naval Postgraduate School Monterey, California 93940	1
19.	Program Director for Meteorology National Science Foundation Washington, D. C.	1
20.	Headquarters 2nd Weather Wing (MAC) United States Air Force APO #633 New York, New York	1

INITIAL DISTRIBUTION LIST (cont'd)

		No. Copies
21.	American Meteorological Society 45 Beacon Street Boston, Massachusetts	1
22.	Commander, Air Weather Service Military Airlift Command U. S. Air Force Scott Air Force Base, Illinois 62226	2
23.	U. S. Department of Commerce, ESSA Weather Bureau Washington, D. C.	2
24.	Commandant of the Marine Corps Navy Department (Code DF) Washington, D. C. 20380	1
25.	Office of Naval Research Department of the Navy Washington, D. C. 20360	1
26.	Chairman Department of Meteorology & Oceanography New York University University Heights, Bronx New York, New York	1
27.	Department of Meteorology University of California Los Angeles, California	1
28.	Department of the Geophysical Sciences University of Chicago Chicago, Illinois	1
29.	Department of Atmospheric Science Colorado State University Fort Collins, Colorado	1
30.	Department of Engineering Mechanics University of Michigan Ann Arbor, Michigan	1

INITIAL DISTRIBUTION LIST (cont'd)

		No. Copies
31.	School of Physics University of Minnesota Minneapolis, Minnesota	1
32.	Department of Meteorology University of Utah Salt Lake City, Utah	1
33.	National Center for Atmospheric Research Boulder, Colorado	1
34.	Department of Meteorology and Climatology University of Washington Seattle, Washington 98105	1
35.	Department of Meteorology University of Wisconsin Madison, Wisconsin	1
36.	Department of Meteorology Florida State University Tallahassee, Florida	1
37.	Department of Meteorology Massachusetts Institute of Technology Cambridge, Mass. 02139	1
38.	Department of Meteorology Pennsylvania State University University Park, Pennsylvania	1
39.	Department of Meteorology San Jose State San Jose, California	1
40.	Hawaii Institute of Geophysics University of Hawaii Honolulu, Hawaii	1
41.	University of Oklahoma Research Institute Norman, Oklahoma	1

		No. Copies
42.	Atmospheric Science Branch Science Research Institute Oregon State College Corvallis, Oregon	1
43.	The University of Texas Electrical Engineering Research Laboratory Engineering Science Bldg. 631A University Station Austin, Texas 78712	1
44.	Department of Meteorology Texas A&M University College Station, Texas 77843	1
45.	Weather Dynamics Group Aerophysics Laboratory Stanford Research Institute Menlo Park, California	1
46.	Meteorology International, Inc. P. O. Box 1364 Monterey, California 93940	1
47.	The Travelers Research Center, Inc. 650 Main Street Hartford, Connecticut	1
48.	United Air Lines Director of Meteorology P. O. Box 8800 Chicago, Illinois	1
49.	Meteorology Section Aracon Geophysics Co. Virginia Road Concord, Massachusetts 01742	1
50.	Librarian GCA Technology Division GCA Corporation Bedford, Massachusetts 01730	1

		No. Copies
51.	Department of Meteorology University of Melbourne Grattan Street Parkville, Victoria Australia	1
52.	Bureau of Meteorology Department of the Interior Victoria and Drummond Streets Carlton, Victoria Australia	1
53.	C. S. I. R. O. Division of Meteorological Physics Station Street Aspendale, Victoria Australia	1
54.	Institut f. Meteor. u. Geophysik Universitat Innsbruck Schopfstrassee 41, Innsbruck Austria	1
55.	Department of Meteorology McGill University Montreal, Canada	1
56.	Central Analysis Office Meteorological Branch Regional Adm. Building Inter. Airport Dorval, Quebec, Canada	1
57.	Meteorological Office 315 Bloor Street West Toronto 5, Ontario, Canada	1
58.	Department of Meteorology University of Copenhagen Copenhagen, Denmark	1
59.	Institute of Meteorology University of Helsinki Helsinki - Porthania, Finland	1

		No. Copies
60.	Institut fur Theoretische Meteorologie Freie Universitat Berlin Berlin-Dahlem Thiel-allea 49 Federal Republic of Germany	1
61.	Meteorological Institute University of Thessaloniki Thessaloniki, Greece	1
62.	Meteorological Service 44, Upper O'Connell Street Dublin 1, Ireland	1
63.	Department of Meteorology The Hebrew University Jerusalem, Israel	1
64.	Geophysical Institute Tokyo University Bunkyo-ku Tokyo, Japan	1
65.	Meteorological Research Institute Kyoto University Kyoto, Japan	1
66.	Department of Astronomy and Meteorology College of Liberal Arts and Sciences Seoul National University Ibng Soong Dong, Chong No Ku Seoul, Korea	1
67.	Central Meteorological Office I Song Wul Dong, Sudaemon Ku Seoul, Korea	1
68.	Department of Meteorology Instituto de Geofisica Universidad Nacional de Mexico Mexico 20, D. F., Mexico	1
69.	New Zealand Meteorological Service P. O. Box 722 Wellington, G. E. New Zealand	1

		No. Copies
70.	Institutt for Teoretisk Meteorologi University of Oslo Blindern, Oslo, Norway	1
71.	Institute of Geophysics University of Bergen Bergen, Norway	1
72.	Pakistan Meteorological Department Institute of Meteorology and Geophysics Karachi, Pakistan	1
73.	Royal Swedish Air Force M. V. C. Stockholm 80, Sweden	1
74.	Department of Meteorology Imperial College of Science South Kensington London S.W. 7, United Kingdom	1
75.	Meteorological Office London Rd. Bracknell Berkshire, United Kingdom	1
76.	National Research Institute for Mathematical Sciences C. S. I. R. P. O. Box 395 Pretoria, Union of South Africa	1

UNCLASSIFIED

Security Classification

DOCUMENT CONTROL DATA - R&D

(Security classification of title, body of abstract and indexing annotation must be entered when the overall report is classified)

1. ORIGINATING ACTIVITY *(Corporate author)*
U. S. Naval Postgraduate School
Monterey, California

2a. REPORT SECURITY CLASSIFICATION
Unclassified

2b. GROUP

3. REPORT TITLE STATIC STABILITY AS AN AID IN NUMERICAL BAROCLINIC-ZONE ANALYSIS

4. DESCRIPTIVE NOTES *(Type of report and inclusive dates)*
Master of Science Thesis (Meteorology)

5. AUTHOR(S) *(Last name, first name, initial)*
Hamrick, James M., Lieutenant, U. S. Navy

6. REPORT DATE	7a. TOTAL NO. OF PAGES	7b. NO. OF REFS
May 1966	92	11

8a. CONTRACT OR GRANT NO.	9a. ORIGINATOR'S REPORT NUMBER(S)
b. PROJECT NO.	
c.	9b. OTHER REPORT NO(S) *(Any other numbers that may be assigned this report)*
d.	

10. AVAILABILITY/LIMITATION NOTICES
This document has been approved for public release and sale; its distribution is unlimited.
Qualified requesters may obtain copies of this report from DDC
GWH 9/15/69

11. SUPPLEMENTARY NOTES	12. SPONSORING MILITARY ACTIVITY
	Chief of Naval Operations (OP-09B7) Department of the Navy Washington, D. C. 20360

13. ABSTRACT

Static stability is investigated as a contribution to numerical baroclinic-zone analysis, developed by Renard and Clarke, and presently being produced on a hemispheric basis by the U. S. Navy at the Fleet Numerical Weather Facility, Monterey, California (FNWF). Significant level and mandatory-level data from the North American region at 00Z and 1200Z, 20 August 1965, are utilized in an experiment relating 850,700,500, and 300-mb static stabilities and associated parameters to a FNWF front-location parameter proportional to horizontal shear of the thermal wind which is dependent on mandatory level data only.

Three methods are used to compute static stability in the form of $\frac{\partial^2 \theta}{\partial p^2}$, the most promising one involving a parabolic fit of potential temperature to the four mandatory levels. A derivative of static stability is used to locate baroclinic zone boundaries. Finally, the vertical gradient of potential temperature in combination with the slope of isentropic surfaces is used to determine isobaric gradients of potential temperature which yields an analysis of baroclinicity with resolution surpassing that of the present FNWF product.

DD FORM 1 JAN 64 1473

UNCLASSIFIED

Security Classification

14. KEY WORDS	LINK A		LINK B		LINK C	
	ROLE	WT	ROLE	WT	ROLE	WT
Static Stability						
Baroclinic Zone						
Numerical Frontal Analysis						
Significant Level Data						

INSTRUCTIONS

1. ORIGINATING ACTIVITY: Enter the name and address of the contractor, subcontractor, grantee, Department of Defense activity or other organization *(corporate author)* issuing the report.

2a. REPORT SECURITY CLASSIFICATION: Enter the overall security classification of the report. Indicate whether "Restricted Data" is included. Marking is to be in accordance with appropriate security regulations.

2b. GROUP: Automatic downgrading is specified in DoD Directive 5200.10 and Armed Forces Industrial Manual. Enter the group number. Also, when applicable, show that optional markings have been used for Group 3 and Group 4 as authorized.

3. REPORT TITLE: Enter the complete report title in all capital letters. Titles in all cases should be unclassified. If a meaningful title cannot be selected without classification, show title classification in all capitals in parenthesis immediately following the title.

4. DESCRIPTIVE NOTES: If appropriate, enter the type of report, e.g., interim, progress, summary, annual, or final. Give the inclusive dates when a specific reporting period is covered.

5. AUTHOR(S): Enter the name(s) of author(s) as shown on or in the report. Enter last name, first name, middle initial. If military, show rank and branch of service. The name of the principal author is an absolute minimum requirement.

6. REPORT DATE: Enter the date of the report as day, month, year; or month, year. If more than one date appears on the report, use date of publication.

7a. TOTAL NUMBER OF PAGES: The total page count should follow normal pagination procedures, i.e., enter the number of pages containing information.

7b. NUMBER OF REFERENCES: Enter the total number of references cited in the report.

8a. CONTRACT OR GRANT NUMBER: If appropriate, enter the applicable number of the contract or grant under which the report was written.

8b, 8c, & 8d. PROJECT NUMBER: Enter the appropriate military department identification, such as project number, subproject number, system numbers, task number, etc.

9a. ORIGINATOR'S REPORT NUMBER(S): Enter the official report number by which the document will be identified and controlled by the originating activity. This number must be unique to this report.

9b. OTHER REPORT NUMBER(S): If the report has been assigned any other report numbers *(either by the originator or by the sponsor)*, also enter this number(s).

10. AVAILABILITY/LIMITATION NOTICES: Enter any limitations on further dissemination of the report, other than those imposed by security classification, using standard statements such as:

(1) "Qualified requesters may obtain copies of this report from DDC."

(2) "Foreign announcement and dissemination of this report by DDC is not authorized."

(3) "U. S. Government agencies may obtain copies of this report directly from DDC. Other qualified DDC users shall request through _____."

(4) "U. S. military agencies may obtain copies of this report directly from DDC. Other qualified users shall request through _____."

(5) "All distribution of this report is controlled. Qualified DDC users shall request through _____."

If the report has been furnished to the Office of Technical Services, Department of Commerce, for sale to the public, indicate this fact and enter the price, if known.

11. SUPPLEMENTARY NOTES: Use for additional explanatory notes.

12. SPONSORING MILITARY ACTIVITY: Enter the name of the departmental project office or laboratory sponsoring *(paying for)* the research and development. Include address.

13. ABSTRACT: Enter an abstract giving a brief and factual summary of the document indicative of the report, even though it may also appear elsewhere in the body of the technical report. If additional space is required, a continuation sheet shall be attached.

It is highly desirable that the abstract of classified reports be unclassified. Each paragraph of the abstract shall end with an indication of the military security classification of the information in the paragraph, represented as *(TS), (S), (C), or (U)*.

There is no limitation on the length of the abstract. However, the suggested length is from 150 to 225 words.

14. KEY WORDS: Key words are technically meaningful terms or short phrases that characterize a report and may be used as index entries for cataloging the report. Key words must be selected so that no security classification is required. Identifiers, such as equipment model designation, trade name, military project code name, geographic location, may be used as key words but will be followed by an indication of technical context. The assignment of links, roles, and weights is optional.